2019

Ice Flow Impacts the Firn Structure of Greenland's Percolation Zone

Rosemary C. Leone
University of Montana, Missoula

ICE FLOW IMPACTS THE FIRN STRUCTURE OF GREENLAND'S PERCOLATION ZONE

By

ROSEMARY CLAIRE LEONE

Bachelor of Science, Colorado School of Mines, Golden, CO, 2015

Thesis

presented in partial fulfillment of the requirements
for the degree of

Master of Science
in Geosciences

The University of Montana
Missoula, MT

December 2019

Approved by:

Scott Whittenburg, Dean of The Graduate School
Graduate School

Dr. Joel T. Harper, Chair
Department of Geosciences

Dr. Toby W. Meierbachtol
Department of Geosciences

Dr. Jesse V. Johnson
Department of Computer Science

Leone, Rosemary, M.S, Fall 2019 *Geosciences*

Ice Flow Impacts the Firn Structure of Greenland’s Percolation Zone

Chairperson: Dr. Joel T. Harper

One dimensional simulations of firn evolution neglect horizontal transport as the firn column moves down slope during burial. This approach is justifiable near Greenland's ice divide, where ice flow is near vertical, but fidelity is lost in the percolation zone where horizontal ice flow advects the firn column through climate gradients. We simulate firn evolution processes under advection conditions using a transient, thermo-mechanically coupled model for firn densification and heat transfer with various schemes for meltwater penetration and refreezing. The simulations isolate processes in synthetic runs and investigate an ice core site and four transects of Greenland’s percolation zone. The impacts of advection on the development of firn density, temperature, and stratigraphy of melt features are quantified, and two dimensional simulations are compared against a 1D baseline. The advection process tends to increase the pore close off depth, reduce the heat content, and decrease the frequency of melt features with depth, by emplacing firn sourced from higher locations under increasingly warm and melt-affected surface conditions. Pore close off and temperature are mainly impacted in the lowermost 20 km of the percolation zone, the impacts vary around the ice sheet but can change the firn’s air content by 10s of percent. Ice flow can also have a substantial impact on the stratigraphy of melt features in the firn column, independent of changing melt frequency, even in locations where the air content and firn temperature are relatively unaffected by advection. Thus, this effect should be quantified in order to correctly interpret temporal changes in ice cores in regards to climate.

Table of Contents

Acknowledgements

I would like to thank my advisor Dr. Joel Harper, who has invested hours helping me grow as a scientist and provided the critical feedback needed for my thesis to develop over the past two years. I would also like to thank my committee members Toby Meierbachtol and Jesse Johnson who have collaborated, discussed ideas with me, and answered any questions I had.

I would also like to thank my officemates at QSSI who have provided emotional support and engagement in intellectual discussions regarding dogs wearing pants. I would like to especially thank Jimmy Stauder and Jake Downs who developed the Greenland tool kit allowing me to map velocity flow lines and were always available to answer programming questions.

I am also grateful for the support from my family and friends who have listened to me talk about firn for the past two years. Lastly, and most importantly, I want to thank my cat Patches who was kind enough to leave multiple presents for me in my room after I came back from my field session in Greenland.

This research was supported by NSF Grants 1717241 and Montana NASA Space Grant Fellowship.

1. Introduction

1.1 The Percolation Zone

The Greenland Ice Sheet (GrIS) covers an area of 1.7×10^6 km^2 occupying much of the land area above the Arctic Circle. About 90% of GrIS is a region of accumulation where annual snowfall exceeds losses to melt and sublimation (Ettema et al., 2009). Layers of snow accumulate each year on top of one another, with deeply buried layers eventually transforming into glacial ice. The aged and compacted snow is called firn and forms a porous column up to 80 m thick (Herron & Langway, 1980). During summer, firn at the highest elevations remains frozen, but approximately 50-80% of the ice sheet experiences some amount of summer melting at the surface (Fettweis et al., 2011). The melting region of the accumulation area is called the percolation zone because the surface melt is known to 'percolate' into the underlying column of firn.

The density and thermal structure of firn within the percolation zone evolves from compaction processes and meltwater infiltration and refreezing. Meltwater can either runoff from the ice sheet, or it can infiltrate into deep and/or shallow layers of the firn column causing a redistribution of mass. When meltwater refreezes, the release of latent heat causes warming of the firn. Firn compaction is highly temperature sensitive due to the Arrhenius-type dependence of densification rate on temperature. Therefore the refreezing of meltwater and firn compaction are strongly coupled processes (Li & Zwally, 2002).

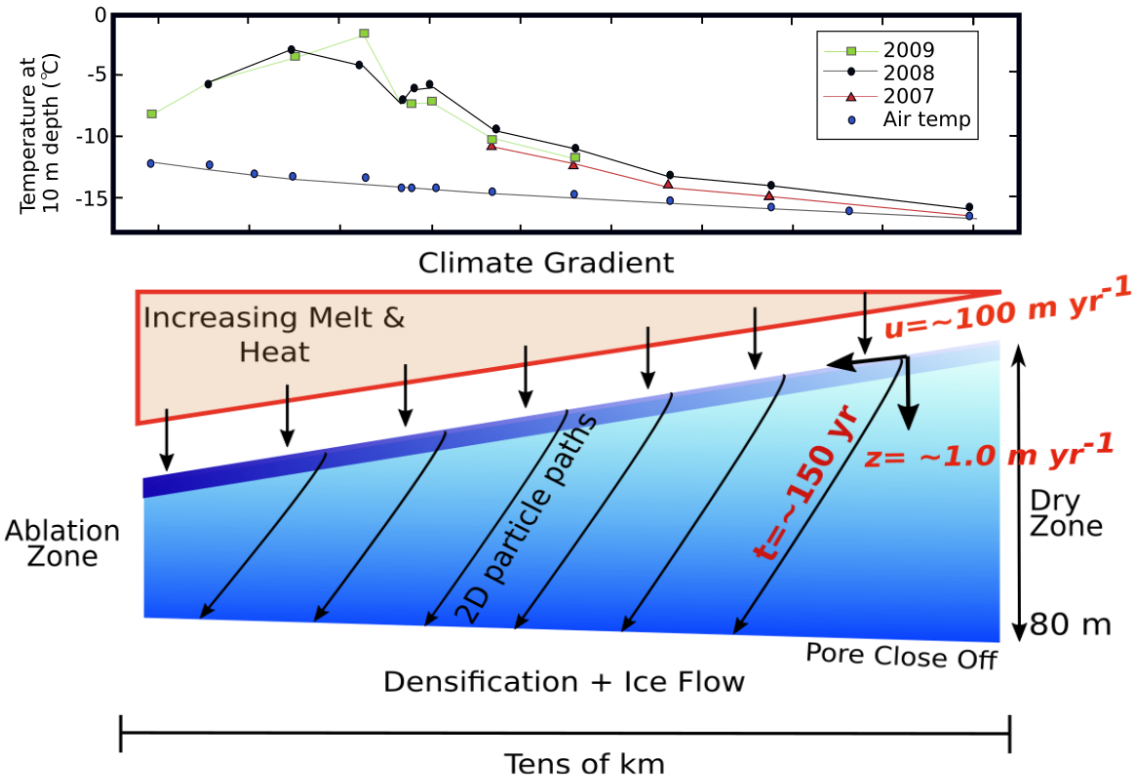

Figure 1. 2D conceptual framework of the percolation zone. Densification, ice flow, and climate gradients are all inextricably coupled. Top panel illustrates spatial climate gradients as represented by air temperature changes (blue dots) and coupled air temperatures and melt changes as represented by 10 m temperatures (green, red, black dots). Figure adapted from (Humphrey et al. 2012).

The density and thermal structure of the column of firn across the percolation zone is not well constrained but should have strong spatial gradients. Higher in the percolation zone, firn compaction is driven by dry firn processes and the complications that arise from meltwater are limited. In the lower elevations of the percolation zone, firn compaction is driven by the formation of ice lenses in addition to an increase in surface temperature and seasonal melt rates. Superimposed on this spatial gradient are temporal changes in melt, refreezing and compaction, both due to interannual variability and an Arctic warming trend. Figure 1 illustrates the spatial gradients in melt and temperature.

1.2 Prior Work

1.2.1 Firn Models

With observations limited, model simulations are the primary tool for investigating the density and thermal structure of the full firn layer. To date, numerical models of firn evolution all consider only 1D profiles. Forced by accumulation rate, initial snow density, and mean surface temperature, they simulate firn compaction and produce depth-density and temperature profiles. Most firn models run to steady state conditions (e.g., Herron & Langway, 1980), although several modeling attempts do consider forcing by transient inputs (Arthern et al., 2010; Simonsen et al., 2013; Zwally & Li, 2002).

The impact of meltwater infiltration has been considered in transient and steady state models (Ligtenberg et al., 2011; Reeh et al., 2005; Simonsen et al., 2013; Steger et al., 2017) but only in a 1D framework with varying ranges of complexity. Reeh et al. (2005) assumes all meltwater refreezes in the annual layer. Other models use the standard tipping bucket method (e.g. Ligtenberg et al., 2011), which allows meltwater infiltration beyond the annual layer when cold content and irreducible water content thresholds are met. More complex models simulates the physics for meltwater flow based on Darcy's Law (e.g. Meyer & Hewitt, 2017).

1.2.2 Observations

Observations of firn density and temperature are mostly in the upper percolation zone or the top 10 m. Studies at two locations high in the percolation zone where melt is quite limited, showed the depth variability of density generally followed firn densification theory, with thin ice layers representing temporal climate variations (Higgins, 2012; Kameda et al., 1995). Limited observations in the upper 10 m show open pore space steadily decreasing with elevation, eventually promoting horizontal runoff (Harper et al., 2012). The resulting firn has open pore

space intermixed with ice layers, ice lenses, and vertical ice pipes (Braithwaite et al., 1994; Pfeffer et al., 1991). Recent data also show that a perennial aquifer of liquid water exists in select locations (Forster et al., 2014).

The thermal conditions of the percolation zone are influenced by meltwater infiltration. Latent heat release from meltwater refreezing causes firn at 10m depth, the approximate depth at which seasonal swings in temperature dissipate, to be warmer than the mean annual surface temperature (Humphrey et al., 2012). There are no measurements to interpolate the deep thermal structure. However, the deep thermal structure should reflect climate variations from decades up to one-to-two centuries, resulting in variable cold content.

There are few studies that have attempted to delineate the structure of the deep firn in the percolation zone. As mentioned above, limited observations have been mainly restricted to shallow (10m or less) depths. Observations show spatial gradients cause significant variance in shallow pore space but the deep pore space remains unknown. Deep observations of the firn density structure are highly limited due to the difficulty and limited incentive to drill in the mixed firn/ice wet medium. One key study used geophysical inversion of radar data (Brown et al., 2012) to estimate the density-depth structure, and concluded that the depth to pore close off in high elevation areas was consistent with dry firn models, but at an intermediate elevation the thickness of the firn layer decreased abruptly for unknown reasons.

Prior work on advection on the Greenland Ice Sheet has been extremely limited. Kameda (1995) modified for ice flow in their ice core interpretations. They analyzed relationships between annual melt thickness and monthly June of temperatures at Jakobshavn and obtained a linear regression with an r value of 0.49. Deviations of the temperature from Jakobshavn were calculated and corrected for the apparent temperature decrease along the core at depth due to ice

flow. They assumed an ice velocity of 38.4 m yr^{-1} and ice sheet slope of 0.20º. The corrections were found to be +0.21º C at 100 m depth and +0.45º C at 206 m. To our knowledge, no other prior work has assessed the impacts of horizontal advection related to ice flow on deep firn structure in the percolation zone. However, this has the potential to be a key process in the development of the deep firn structure.

1.2.3 Ice Cores in the Percolation Zone

Until recently, ice cores from the Greenland Ice Sheet were only studied from the dry snow zone. However, increase mass loss of the GrIS has created a need to study past climatic conditions in order to investigate if the climatic warming we are experiencing is unprecedented. Ice cores from the percolation zone attempt to look at melt features in order extrapolate past summer temperatures. Firn cores in the percolation zone are a complex representation of the past combined with both temporal and spatial gradients. However, no previous study has taken into account advection when quantifying past climatic conditions.

Ice cores from the percolation zone can be divided into melt features and dry polar firn. Melt features can be distinguished due to their brighter appearance and low bubble concentration (Kameda et al., 1995). Melt layers form during summer months when incoming solar radiation causes a portion of the annual snow layer to melt. In order to compare how melt has changed from year to year, the Melt Feature Percentage (MFP) for each annual layer is computed. MFP is the percentage of the annual firn layer composed of refrozen meltwater and can be calculated by visually identifying annual layers or using isotopic dating.

The unclear fate of meltwater makes it difficult to correctly identify the annual MFP. Meltwater can either runoff from the ice sheet, infiltrate into deep and/or shallow layers of the firn column or form perennial firn aquifers (Forster et al., 2014; Koenig et al., 2014). Field

observations suggest a significant amount of meltwater penetrates past 10 m (Humphrey et al., 2012). Field results also indicate the presence of piping events in the percolation zone, where meltwater can travel through impermeable ice layers through a vertical breakthrough channel which causes large heterogeneity of the firn column (Humphrey et al., 2012). Studies attempt to correct for this by applying a multi-year moving average of melt features (Graeter et al., 2018; Higgins, 2012).

Kameda (1995) studied two ice cores from Site J that were 206.6 and 101.5 m deep and observed 2804 melt features. They reconstructed June monthly temperatures by creating a linear regression of MFP versus mean June temperatures at Jakobshavn. They corrected for the decrease in temperature with depth of the core due to ice flow, assuming a velocity of 39.4 m yr^{-1} and ice-sheet slope of 0.20.

MFP was calculated for each 1 m length of the core according to (Koerner, 1977) ice-percentage equation. Koerner (1977) accounts for the differences in the rate of compaction of ice and firn,

$$MFP = \frac{0.9S_i}{0.9S_i + \rho_f S_f} \quad (1)$$

Where S_i and S_f are the measured cross-sectional areas of ice and firn respectively, added together should equal the cross sectional area of the annual layer. The approximate density of ice is 0.9 (g cm^{-3}) and ρ_f is the density of firn (g cm^{-3}). Annual MFP was then determined using a cubic spline curve. A digital Chebyshev filter was then used to look at long term trends in the annual MFP.

More recently, (Graeter et al., 2018) studied seven firn cores collected from the west GrIS percolation zone at 2,100-2,500 m elevation. They combined their core information with

Site J ice core MFP record (Kameda et al., 1995) (located at a 100 m lower elevation) to extend the data back to 1547. They found that five of the cores showed a significant increase in meltwater over the past 50 years. They did not do any correction for ice flow in their study.

Grater (2018) calculated MFP by identifying annual layers by measuring seasonal oscillations in δO^{18} and concentration of major ions, methanesulphonic acid, and dust. They combined their depth-age curves with core density measurements in order to determine annual accumulation rates. Next they identified ice layers using a light table to measure total thickness of ice layers in each annual layer. They divided annual ice layer thickness by the annual accumulation to obtain MFP. Using a Pruned Exact Linear Time (PELT) changepoint analysis they attempted to identify anomalous large shifts in mean or slope of the MFP.

Trusel (2018) created a 339-year stacked record of Central West Greenland melt from ice cores drilled between 2003-2015. They noted a more frequent and intense melting towards present day with a 250% to 575% increase in melt intensity over the past 20 years. The melt records correlate significantly with summer air temperatures from the Ilulissat region and they found positive correlations with RACMO2 modeled melt, refreezing, and runoff. They assume that the spatial character of melt has remained stationary through time. The reconstructions show a non-linear melt-temperature relationship shown by the intensification of recent melt which is unprecedented for the past 6,800-7,800 years (Trusel et al., 2018).

Trussel (2018) scanned each core with the National Ice Core Laboratory (NICL) high-resolution optical imaging system in order to manually identify refrozen melt layers in each digitally registered core depth. They calculated annual melt as a percentage of annual snow accumulation, converting both to water equivalent lengths. To account for thinning as a function of depth, they followed Kameda (1995).

1.3 Scientific Scope

1.3.1 Problem Statement

Ice sheet motion represents an obstacle to deep firn extrapolation that has not been thoroughly examined. As firn in the percolation zone becomes buried, it migrates downstream relatively quickly, moving to a warmer elevation. For example, under typical conditions of the percolation zone (1% surface slope, 100 m yr^{-1} horizontal velocity, 1.0 m yr^{-1} burial rate due to accumulation), a firn layer now 50 m below the surface at 1600 m elevation originated 150 years prior, at a location 15 km up flow at an elevation of 1750 m (Figure 1). This represents an approximate 1°C increase in temperature and 25% increase of seasonal melting. Therefore, the effects of advection on deep pore space may be substantial but this remains unconstrained.

Modeling and observational shortcomings create critical uncertainties regarding the density and thermal structure of the deep firn layers within the percolation zone. Not even the thickness of the firn column is clear for much of the percolation zone. This results in a critical uncertainty regarding the amount of deep pore space in firn that could absorb future meltwater and latent heat. There have been no attempts to quantify the importance of the 2D effect resulting from horizontal advection of firn as it becomes buried and moves downslope. No current model considers the added effects of infiltration overprinting, mass redistribution and enhanced compaction rates due to release of latent heat. The purpose of this research is to test the 2D effects on firn densification in order to constrain the volume, and the temperature/density structure of Greenland's melting firn layer.

1.3.2 Broader Implications

The percolation zone is potentially a major storage reservoir for meltwater generated on the surface of the GrIS (Harper et al., 2012; Pfeffer et al., 1991). It is estimated that the

percolation zone could have 322-1289 Gt of storage capacity (Harper et al., 2012). On the other hand, thick ice layers can route meltwater into runoff (Machguth et al., 2016). GrIS currently contributes 0.21-0.74 mm yr^{-1} to global sea level rise and is an increasing contributor to sea level due to stronger surface melt (Ettema et al., 2009). The structure and long term fate of deep pore space is unclear, but may play an important role in meltwater retention/runoff processes, and cannot necessarily be determined from shallow observations only. Meltwater refreezing within the extensive area of the percolation zone transfers substantial heat from the atmosphere to the ice sheet, thus having far reaching impacts on other Arctic climate systems including the oceans and sea ice. With increased runoff there is potential for ocean freshening, potentially influencing ocean circulation patterns across the Northern Hemisphere.

2. Methods

2.1 Model Description

2.1.1 Firn Densification

The density and thermal structure of firn within the percolation zone is a function of temperature, accumulation rate, and melt rates (e.g. Herron & Langway, 1980, Reeh et al., 2005). The spatial gradients in these parameters, coupled with the speed at which the ice moves through the spatially variable climate, determines the influence of ice flow on deep firn structure. We quantify this effect using a transient, thermo-mechanically coupled model for firn densification and heat transfer that includes meltwater penetration and refreezing.

The densification of firn is divided into three stages (Figure 2). The first stage, above 550 kg m^{-3}, densification occurs at a faster rate and is mainly due to grain settling and packing. Between 550-830 kg m^{-3} densification occurs at a slower rate and the main processes are

sublimation, diffusion, and deformation of the snow grains. After 830 kg m^{-3} the pore close off zone is reach where air can no longer leave or exit the grains and densification into ice is dominated by compression of the air bubbles (Herron & Langway, 1980).

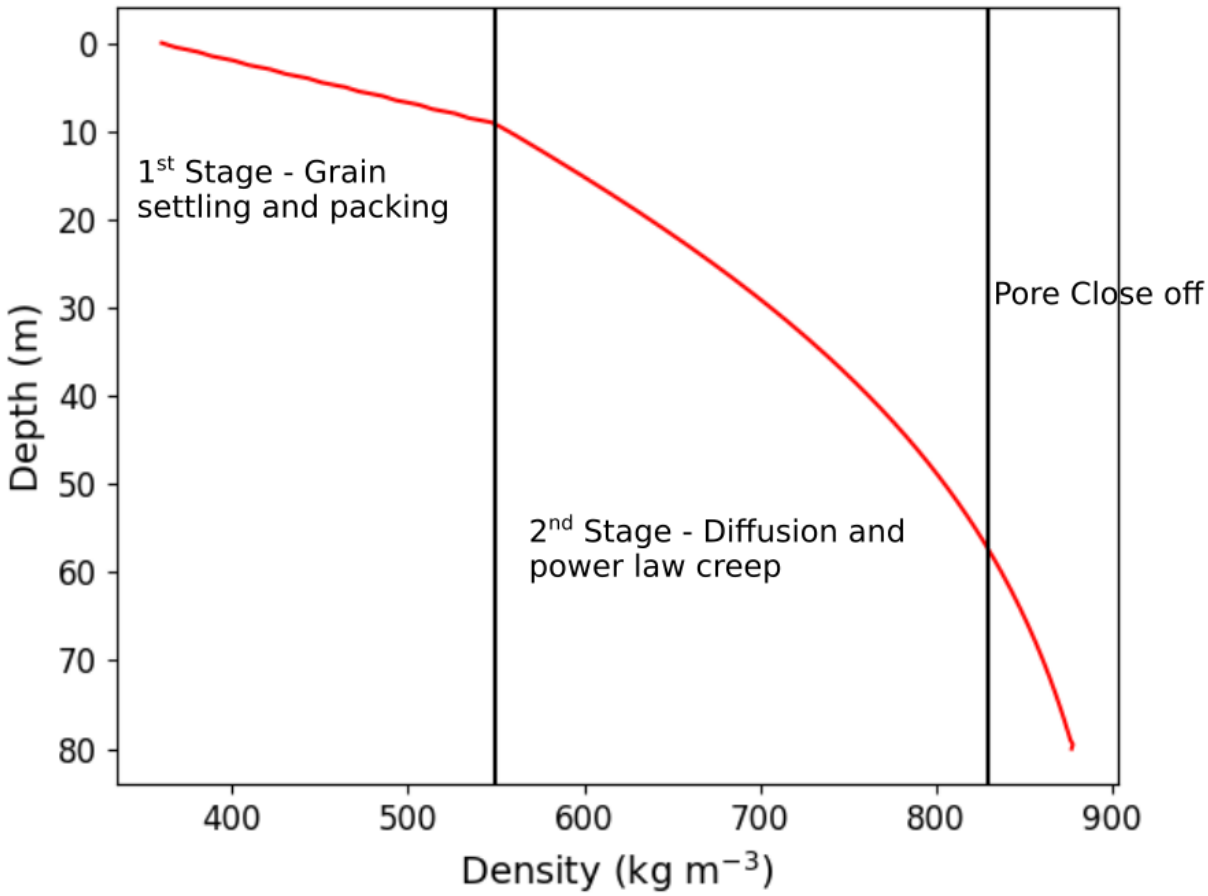

Figure 2. Standard firn density curve divided into the three stages of densification.

We chose to use The Herron and Langway (HL) firn densification model (1980) for simplicity. We find the HL model density and temperature results matches well with other more complex firn models. For more information see Appendix A. The HL model is empirically constructed based on the assumption that 'the proportional change in air space during densification is linearly related to the change in stress due to the weight of the overlying snow'

(Robin, 1958). The rate of densification changes for the first two stages of firn densification and is tuned by a constant *c,* which was determined by depth-density data from Greenland and Antarctica. These data were plotted based on the ratio of the natural log of $\rho/(\rho_i-\rho)$ versus depth, where ρ is the density of firn and ρ_i is the density of ice. Using a steady state assumption, the model describes the annual 'increase of stress due to the overlying snow' as the annual accumulation rate. The accumulation rate dependency varies exponentially by an empirically derived constant from the slope of the line $\ln[\rho/(\rho_i-\rho)]$. The densification rate is then assumed to have an Arrhenius-type temperature dependence.

$$\frac{d\rho}{dt} = \begin{cases} c_0(\rho_i - \rho) \; if \; \rho \leq \rho_c \\ c_1(\rho_i - \rho) \; if \; \rho_c < \rho \end{cases} \tag{2}$$

Where ρ_c is defined as 550 kg m^{-3} and c_0 and c_1 are defined as

$$\begin{cases} c_0 = 11bexp\left(\frac{-10160}{RT}\right) \text{ if } \rho \leq \rho_c \\ c_1 = 575b^{0.5}exp\left(\frac{-21400}{RT}\right) \text{ if } \rho_c < \rho \end{cases} \tag{3}$$

Where R is the gas constant (8.314 J K^{-1} mol^{-1}) and accumulation rate b is in water equivalent units. We use an initial snow density of 360 kg m^{-3} for the top boundary condition and an initial vertical velocity of $(b*\rho_i/\rho)$, for an accumulation rate b (meters of ice added to the surface per year).

2.1.1.2 Firn Air Content

The capacity of the percolation zone to store meltwater can be quantified as the firn air content. The firn air content represents the maximum amount of infiltration meltwater the firn column could hold. First the 'load' profile of the firn column is calculated by integrating firn

density with respect to depth. We then take the difference between the load profile of the firn column and of the 'ice capacity' or the maximum amount of meltwater that could possibly be stored in the firn (Harper et al., 2012). We used an average density of 843 kg m^{-3} for infiltration ice as in Harper (2012). This results in the following equation

$$C(z) = \int_0^z \left(\rho_{ii} - \rho(\zeta)\right) d\zeta \tag{4}$$

where ρ is firn density and ρ_{ii} is the infiltration ice density. This capacity calculation does not take into account perennial firn aquifers where capacity must be adjusted by 8.9% due to density differences between water and ice (Koenig et al., 2014). In order to obtain meters of air content of ice (and thus avoiding the complications that arise between the differences of water and ice density) we divide the total capacity by the density of ice.

2.1.2 Temperature Evolution

Firn temperature was modeled by solving the standard one-dimensional time-dependent heat-transfer equation with latent heat from the refreezing of meltwater (Paterson, 1994).

$$\rho c_i \frac{\partial T}{\partial t} = k_T \frac{\partial^2 T}{\partial z^2} + \left[\frac{dk_T}{dz} - \rho c \omega\right] \frac{\partial T}{\partial z} + S \tag{5}$$

Where ρ is density, c_i heat capacity, k_i thermal conductivity, ω vertical velocity, T temperature of the firn, and S as sources and sinks. We used thermal conductivity of firn as described in (Arthern & Wingham, 1998) and a constant heat capacity for simplification. Thermal conductivity of the firn is defined as (Arthern & Wingham, 1998).

$$k_i = 2.1 \left(\frac{\rho}{\rho_i}\right)^2 \tag{6}$$

We use a constant boundary condition at the surface based on the annual mean air temperature. The rate of latent heat source is added on as,

$$S_{LH} = L_f \rho_w F \tag{7}$$

Where Lf is the latent heat of fusion (334000 J kg^{-1}), ρ_w is water density, and *F* is the volume fraction per unit time of refrozen meltwater. This is determined based on the melt scheme chosen.

2.1.3 Vertical Velocity

To estimate compaction rates the rate of densification can be integrated with respect to depth and solved for the vertical firn velocity.

$$\omega(z,t) = \int_0^z \frac{1}{\rho(z)} \frac{d\rho(z)}{dt} dz \tag{8}$$

2.1.4 Melt Schemes

Modeling complex and heterogeneous meltwater infiltration in firn is beyond the scope of this project and remains an outstanding research topic of critical importance. Instead, our approach is to implement three different melt schemes (Figure 3) which vary in complexity and reflect a range of states to facilitate reasoning of the role of meltwater infiltration on deep firn structure.

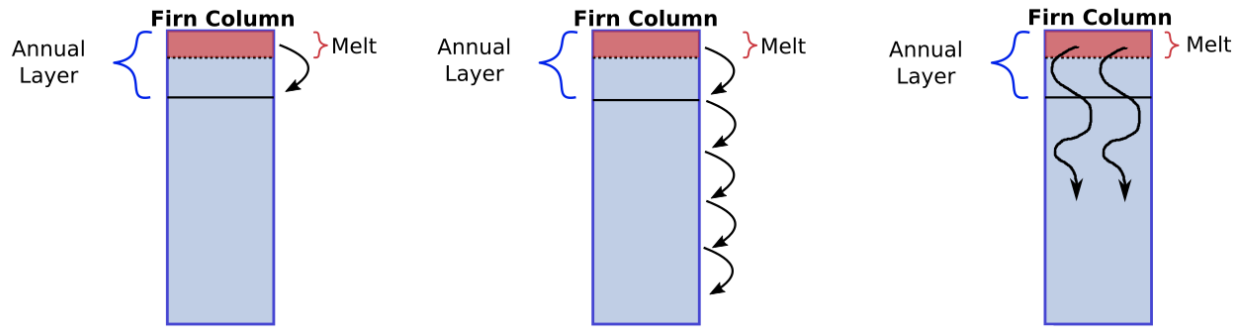

Figure 3. Schematic of the three different melt schemes used in this study. Reeh model (left), tipping bucket model (middle), continuum model (right).

2.1.4.1 Reeh

The first model is limited to shallow infiltration, and assumes that all meltwater refreezes in the annual layer (Reeh et al., 2005). Reeh (2005) created a simple firn densification model following the HL parameterization including shallow meltwater infiltration. Each annual layer is composed of an ice fraction and a firn fraction; assuming the amount of refrozen meltwater does not penetrate past the annual later. The mean density of each layer is calculated by dividing the weight per unit area by the total thickness of the annual layer.

$$\rho = \frac{\rho_{firn}}{1 - \frac{SIR}{b}\left(1 - \frac{\rho_{firn}}{\rho_i}\right)} \tag{9}$$

Where ρ_{firn} is the density of the firn fraction, SIR is the amount of refrozen meltwater, b is the annual accumulation, and ρ_i is the density of ice.

2.1.4.2 Tipping Bucket

The second model implements the standard tipping bucket method (Ligtenberg et al., 2018; Munneke et al., 2014), which allows meltwater infiltration beyond the annual layer when cold content and irreducible water content thresholds are met. Meltwater percolates until it is extinguished (ie. reaches a firn layer with a smaller irreducible water content than liquid water

available), or the pore close off density is reached, in which case remaining meltwater runs off instantaneously.

Each firn layer can hold a certain amount of liquid water defined as the irreducible water content which was calculated as a function of the firn porosity (*P*) (Coléou & Lesaffre, 1998).

$$W = 1.7 + 5.7\frac{P}{(1-P)} \tag{10}$$

Cold content is defined as the amount of liquid water (in m) needed to raise the firn layer from the current temperature to 0° C.

$$CC = [\rho_s c_i dT_s]/(\rho_w L_f) \tag{11}$$

Where ρ_s is density (kg m^{-3}), d is firn layer height (m), T_s is temperature (°C), and L_f is the latent heat of fusion (K kg^{-1}).

The firn column was broken up into discrete 10 cm thick layers. The meltwater infiltrates into the firn by tipping from one layer to the next, within one time step, density and temperature are updated at the end of the time step. The meltwater is tipped from one layer to the next and is distributed based on cold content and pore space.

2.1.4.3 Continuum Model

The third infiltration model implements a continuum approach (Meyer & Hewitt, 2017), which simulates the physics for meltwater flow based on Darcy's Law, and treats both saturated and unsaturated conditions.

$$\phi S(u_w - u_i) = \frac{-k(\phi)}{\mu} k_r(S)(\nabla p_w + \rho_w g\hat{z}) \tag{12}$$

Where ϕ is porosity, S is saturation or fraction of void space filled with water, u_w and u_i are the velocities of water and ice respectively, p_w is the water pressure, $k(\phi)$ is the permeability, $k_r(S)$ is the relative permeability, and μ is the viscosity of water. permeability, a simplified Carman-Kozeny relationship is used, given by,

$$k(\phi) = \frac{d_p^2}{180}\phi^3 = k_0\phi^3 \tag{13}$$

where d_p is a typical grain size.

When the firn is unsaturated, flow is driven by capillary forces. Water pressure is related to capillary pressure assuming the air pressure is zero. The capillary pressure and relative permeability are then functions of the saturation. For saturated firn, water pressure is governed by mass conservation. The equations are modified for one dimensional water flow and the variables are changed into a frame that moves with the ice surface.

2.1.5 2D Model Formulation

2.1.5.1 Explicit Two Dimensional Approach

Temperature, density, and vertical velocity were coupled together and solved using the finite element library FEniCS with Galerkin's method and an explicit time step. FeniCS is an open-source computing platform used to solve partial differential equations. Dirichlet boundaries for state variables temperature, density, and vertical velocity are imposed at the model surface, and vertical gradients in these variables are set to 0 at the model base.

An explicit 2D model for densification and heat transport that includes horizontal diffusion was modeled using a two dimensional mesh. 2D particle motion was added by assuming the velocity at the surface is equal to the velocity at depth (the shear deformation in

firn is negligible) and is added into the model as advection by applying the chain rule to the total derivative.

$$\frac{D\rho}{Dt} = \frac{\partial \rho}{\partial t} + \omega \frac{\partial \rho}{\partial z} + u \frac{\partial \rho}{\partial x} \tag{14}$$

Where u corresponds to the horizontal velocity. The temperature equation was also updated in order to include advection terms.

$$\rho c_i \frac{\partial T}{\partial t} = k_T \left(\frac{\partial^2 T}{\partial z^2} + \frac{\partial^2 T}{\partial x^2} \right) - \rho c u \frac{\partial T}{\partial x} + \left[\frac{dk_T}{dz} - \rho c \omega \right] \frac{\partial T}{\partial z} \tag{15}$$

The surface boundary condition for temperature varied by several degrees across the surface domain to simulate the lower elevations of the percolation zone. Various velocities were tested in the absence of melt over the 2D scheme in order to compare the fit between fully 2D and cascading mode.

2.1.5.2 Cascading Approach

In order to increase runtime and include meltwater schemes, we used a pragmatic approach that considers cascading 1D profiles. Profiles simulated higher on the ice sheet inform the initial conditions for locations lower on the ice sheet, as the profiles move to lower elevation. Changing surface conditions as ice flow transports the firn column down-glacier are translated to time-varying boundary conditions using surface velocities (Figure 4). This approach captures the processes of burial, ice layer formation/preservation, and vertical heat transport, but lacks horizontal heat diffusion.

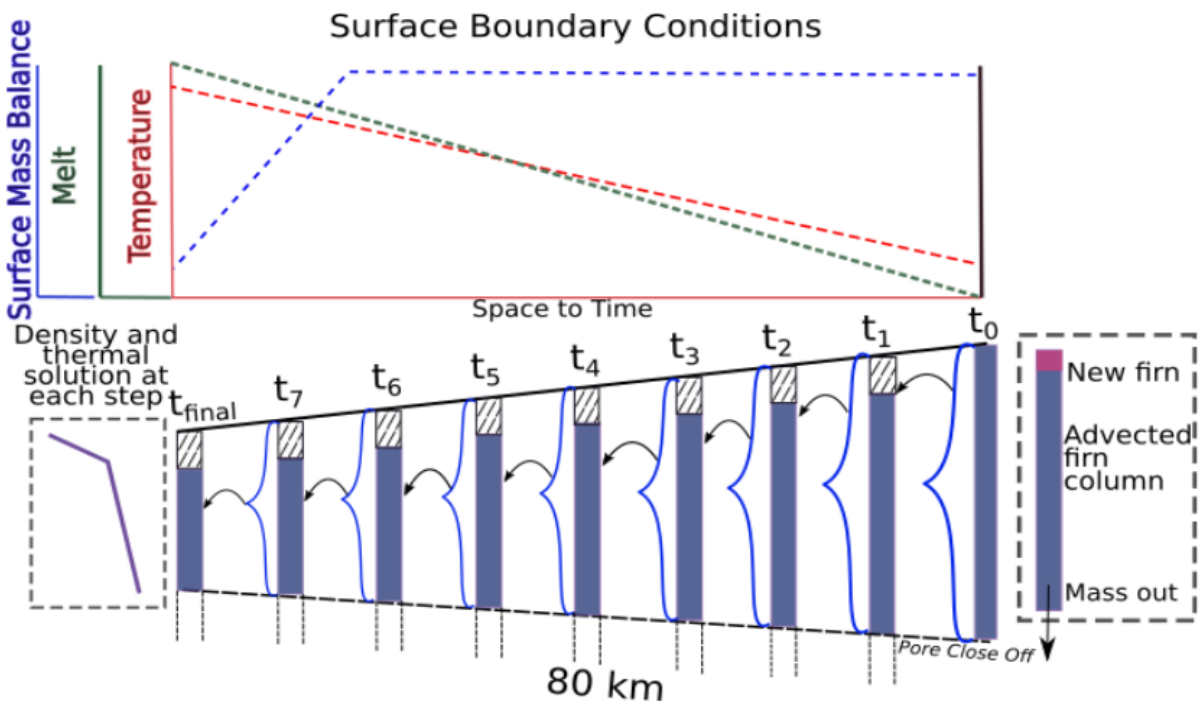

Figure 4. 2D model approach. Changing surface conditions as ice flow transports the firn column down glacier are translated to time-varying boundary conditions using surface velocity. New firn accumulates on top of older firn which originated at a higher elevation. Mass loss occurs at the bottom after firn reaches pore close off.

2.2 Model Experiments

We conducted an initial test of model sensitivity to ice flow and spatial gradients in climate forcings (temperature, melt, and accumulation) in isolation. We then applied the model to four flow-line transects across GrIS' percolation zone spanning a spectrum of expected ice velocities and environmental conditions.

2.2.1 Sensitivity Tests

Synthetic sensitivity tests were performed around a base case scenario with horizontal velocity of 100 m yr^{-1} and an accumulation rate of 0.5 m yr^{-1} ice equivalent. Horizontal velocities were varied from 0 - 500 m yr^{-1}, accumulation rates were varied from 0.1 - 1.0 m yr^{-1} ice equivalent, and total melt was varied from 0 - 85% of the accumulation value from this base case. Total melt represents the amount of melt experienced at the bottom of the percolation zone.

The base case was chosen to loosely match conditions along the EGIG transect, and the ranges of values tested spans the spectrum of conditions that may occur in GrIS' percolation zone. Additionally, we imposed three different surface temperature gradients in each simulation to determine model sensitivity to a spatially varying surface temperature boundary. Simulations were performed for horizontal temperature gradients manifested in surface slopes of 0.3°, 0.6°, 0.8° assuming a temperature lapse rate of -7.4 °C/km (Fausto et al., 2009). We recognize that lapse rates are subject to spatial variability but is a reasonable estimate for this study. These surface slopes are not unreasonable for the GrIS percolation zone (Helm et al., 2014).

We used temperature at pore close off and air content (integrated air space computed as meters of ice) as comparison metrics. Both 2D and 1D model simulations were performed for each sensitivity scenario, and the difference was calculated as

$$\sigma_{\%diff} = \frac{\sigma_{2D} - \sigma_{1D}}{\left(\frac{\sigma_{1D} + \sigma_{2D}}{2}\right)} \tag{16}$$

where σ is the metric of interest.

2.2.2 Greenland Transects

We implement our 2D modeling approach at four test transects spanning the GrIS (Figure 5): 1) the well-studied EGIG transect in western GrIS, 2) a transect feeding Jakobshavn Isbrae, 3) the K-transect in southwest GrIS, and 4) a transect extending from Helheim Glacier. These four study profiles were selected to capture the wide variety of conditions across the ice sheet (Table 1; Figure 6). Surface velocities along study transects were defined from Interferometric Synthetic Aperture Radar (InSAR) data (Joughin et al., 2010) and 1980-2016 average climate variables were selected from RACMO2.3p2 (Noël et al., 2018). This time period was selected to loosely capture the increase in GrIS melt since the late 20th century (Fettweis et al., 2011).

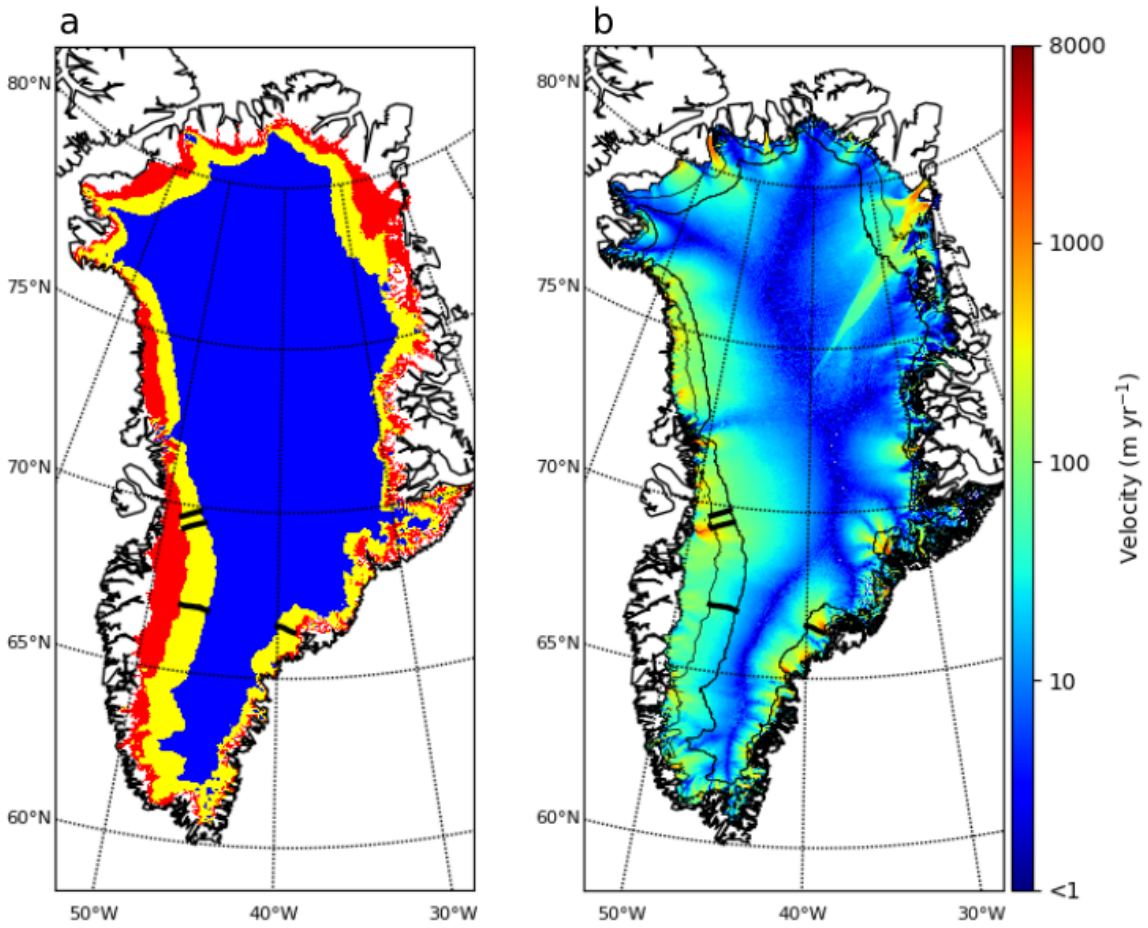

Figure 5. Map of Greenland: Left panel delineating dry snow (blue), percolation zone (yellow), and ablation zone (red) as defined by RACMO 2.3p2 1980-2016. Percolation zone was defined on lower end by areas with accumulation greater than melt and on the upper end by zero latent heat at 10 m depth. Bold black lines represent transects chosen. Right panel showing velocity field overlaid by contour lines of the dry snow, percolation zone, and ablation zone.

Table 1. Conditions along the four transects used in the study.

Transect	EGIG	Jakobshavn	K-transect	Helheim
Elevation Range (m)	1470-1950	1290-2020	1700-2082	1232-2160
Speed (m yr^{-1})	93-150	85-400	27-71	35-1900
Snowfall (m ice equiv)	0.46	0.55	0.4	0.70-1.3
Temperature (ºC)	-14º to -18º	-13º to -18º	-9º to -18º	-15º to -17º
Melt (m ice equiv)	0.11-0.43	0.1-0.53	0.15-0.4	0.1-1.3

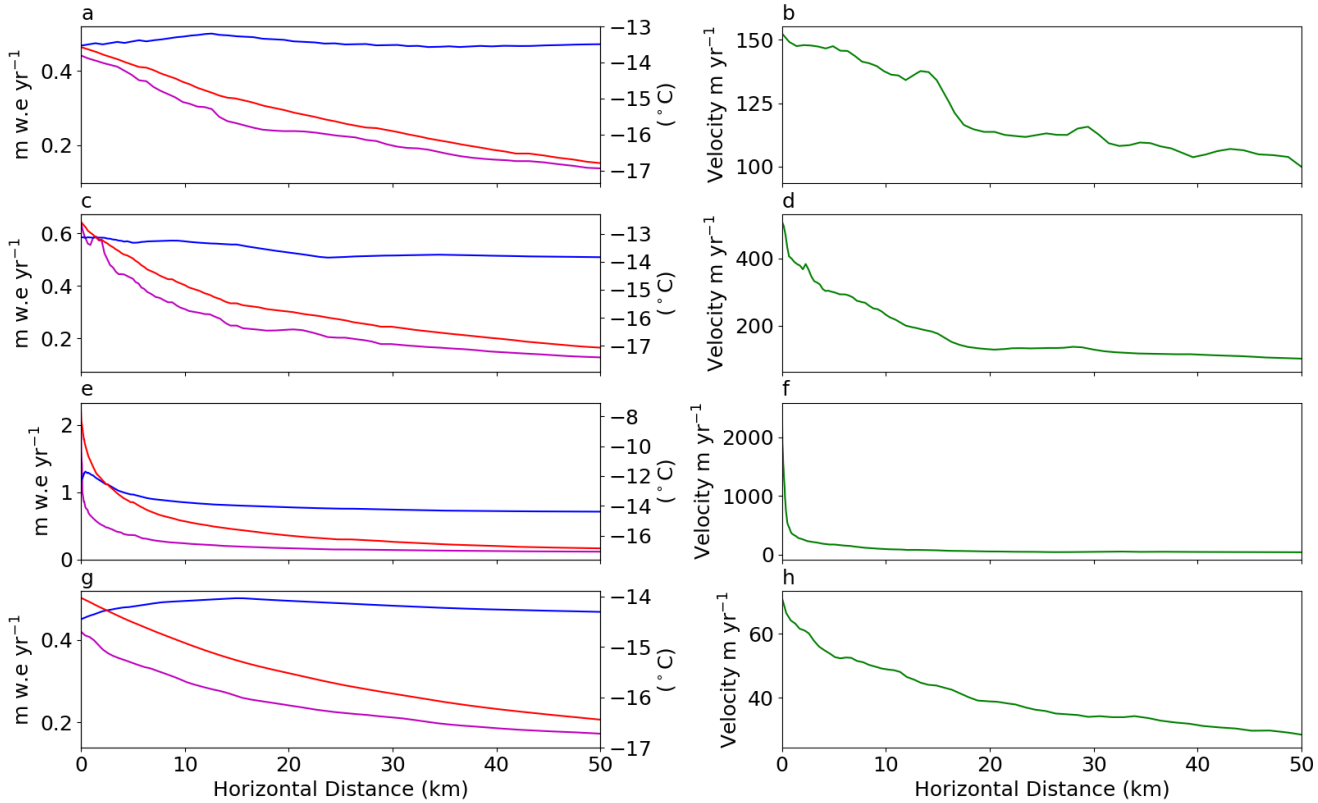

Figure 6. Conditions over the last 50 km for the transects a) EGIG c) Jakobshavn e) Helheim and g) K-transect. Velocities (right panel) for b) EGIG d) Jakobshavn f) Helheim h) K-transect. Blue line represents snowfall, red line represents temperature, magenta line represents melt, and green line represents velocity.

2.3 Quantifying Spatial Influence along EGIG line

In order to quantify the importance of spatial gradients when interpreting a core in the percolation zone we analyzed a 152 m ice core collected in 2007 at Crawford Point by Mosley-Thompson (Higgins, 2012) and a 32 m core drilled by Harper (2018). Mosley-Thompson calculated MFP by overlaying a grid image on top of an image file of the core and counting the cells that contained melt and divided by the total grid cells in each annual layer. Timescales were calculated using variations in δO^{18}. In order to account for differences in depth they applied a density model, which was previously applied to the core, to calculate the percent difference in

each year's average density and then scaled the number of grid cells in the annual layer by the percent difference.

We calculated flow lines up slope from Crawford Point using vertical velocities calculated with a simple Reeh (2005) meltwater model and horizontal velocities from NASA MeaSURES program. Using the Reeh (2005) model we calculated a modeled pore close off depth and age to compare against the observed pore close off depth and age. The flowlines are used to estimate the origin up-flow of the firn at depth and obtain modeled depth and time.

To examine the long term changes and adjust for meltwater that infiltrates past the annual layer, we used the adjusted melt percent calculated by Higgins (2012) and applied a 10-year running mean. We then applied a hamming filter to smooth over the data. This is necessary due to the inhomogeneous method of meltwater infiltration. Therefore, all meltwater refrozen in an annual layer may not have been generated in that year. Next, we subtracted each data point from present day to obtain a ΔMFP to look at long term changes in the core.

To investigate the influence of spatial changes we calculated a 25 km flow line above Crawford Point. Using averaged melt and snowfall values from 1980-2016 from RACMO2.3p2 we estimated how melt and accumulation change up flow on the ice sheet. By using RACMO2.3p2 we are assuming spatial climate gradients are unchanged over a century time scale, where advection of firn from higher elevations with lower ice content reduces the MFP at depth. Using ages calculated from MT core and velocities calculated from NASA MeaSURES Program we integrated over the variable velocity field and associated the spatial MFP with depth along the core and subtracted each data point from Crawford Point RACMO2.3p2 MFP to look at ΔMFP. We used our calculated ΔMFP to obtain annual changes in MFP per year in order to compare with the core results.

3 Results

3.1 Cascading Model Validation

In order to validate the cascading model approach, we tested against the explicit 2D simulation. A comparison between the explicit 2D model and the cascading model following the conditions along the EGIG transect can be seen in Figure 7. We used an accumulation rate of 0.5 m ice equivalent per year, velocity of 100 m yr^{-1}, and a temperature surface boundary condition ranging from -19° to -13° over 90 km. The results show negligible differences between the density curves, with a maximum difference of ~1.4 kg/m^3 at pore close off. Small differences of approximately 0.01° between temperature curves are seen in the cascading versus full 2D approach. This was determined to be due to horizontal conduction which was found to be a negligible difference. We find the maximum error in temperature due to horizontal conductance to be ~0.15° at velocities greater than 1000 m yr^{-1}. This supports our modified approach, which we use for its flexible implementation of melt schemes and its fast runtime.

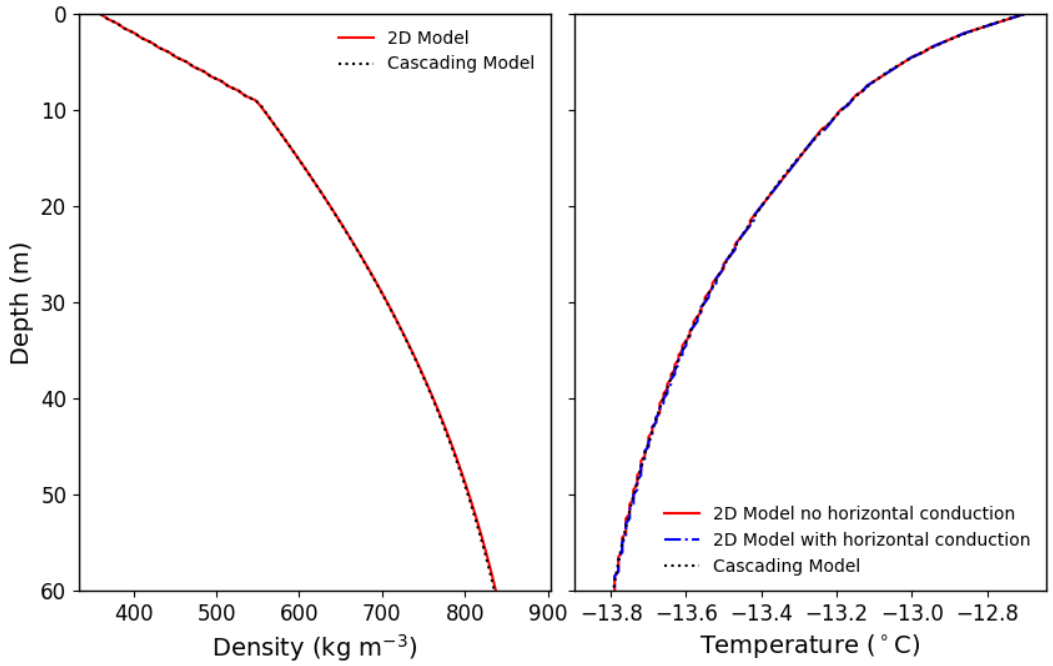

Figure 7. Left: Cascading model compared with full 2D density at 80 km. Right: Cascading model compared with full 2D temperature with and without horizontal conduction

3.2 Sensitivity Tests

Results from the sensitivity tests can be seen in Figure 8. Synthetic model simulations demonstrate the isolated impacts of velocity, accumulation, melt, and slope from 2D-advection. The purely dry scenario, although lacking fidelity for the percolation zone, provides a baseline for revealing the influences of advection and meltwater infiltration on firn evolution.

3.2.1 Influence of Velocity

Increasing the velocity of the firn package exacerbates the effect of 2D-advection in simulations, yielding results that increase air content by 10-20% at slow velocities and up to 80% at high velocities (Figure 8a). Advection results in greater air content and thus depth to pore close off than the 1D model, because higher elevation firn with less melt is transported down

glacier, buried, and preserved at depth. Melt scenarios have a higher effect than the dry model with 2D-advection; the dry model increases air content by only ~15% at the highest velocity. Doubling the velocity from 100 m yr^{-1} to 200 m yr^{-1} increases the effects of advection on air content by approximately 3%, 16%, 7%, and 7% for the dry, Reeh, tipping bucket, and continuum models respectively (Figure 8a).

Faster velocities result in colder temperatures at depth compared to the 1D simulation. The dry scenario reaches a maximum percent difference of ~35%, while the melt scenarios vary from 0-25% at the highest velocity (Figure 8b). The continuum model shows almost no difference in temperature from the 1D. Doubling the velocity from 100 m yr^{-1} to 200 m yr^{-1} increases the effects of advection on temperature at pore close off by approximately 7%, 3%, 4%, and <1% for the dry, Reeh, tipping bucket, and continuum models respectively (Figure 8b).

3.2.2 Influence of Accumulation Rate

For all melt scenarios, smaller accumulations resulted in the largest increase in air content (Figure 8c). Advection is exacerbated due to reduced densification rates under smaller annual increments of overburden, and thus longer preservation of cold and porous firn that becomes deep firn further down-glacier. The influence of accumulation on advection changes most rapidly between 0.1-0.2 m ice equivalent. Doubling from 0.1 to 0.2 m ice equivalent decreases the effects of advection on air content by approximately 1%, 10%, 3% for the dry, Reeh, and tipping bucket models respectively. While doubling from 0.4 to 0.8 decreases the affects by approximately 1.5%, 5%, 2% for the dry, Reeh, and tipping bucket models respectively.

Adding advection to simulations decreases the bulk firn temperature at pore close off in all scenarios except for the tipping bucket model under high accumulations (Figure 8d). Due to

the large amount of melt in these scenarios, run off occurs at pore close off. In the 2D model the pore close off is deeper, thus melt is allowed to percolate further and less latent heat escapes.

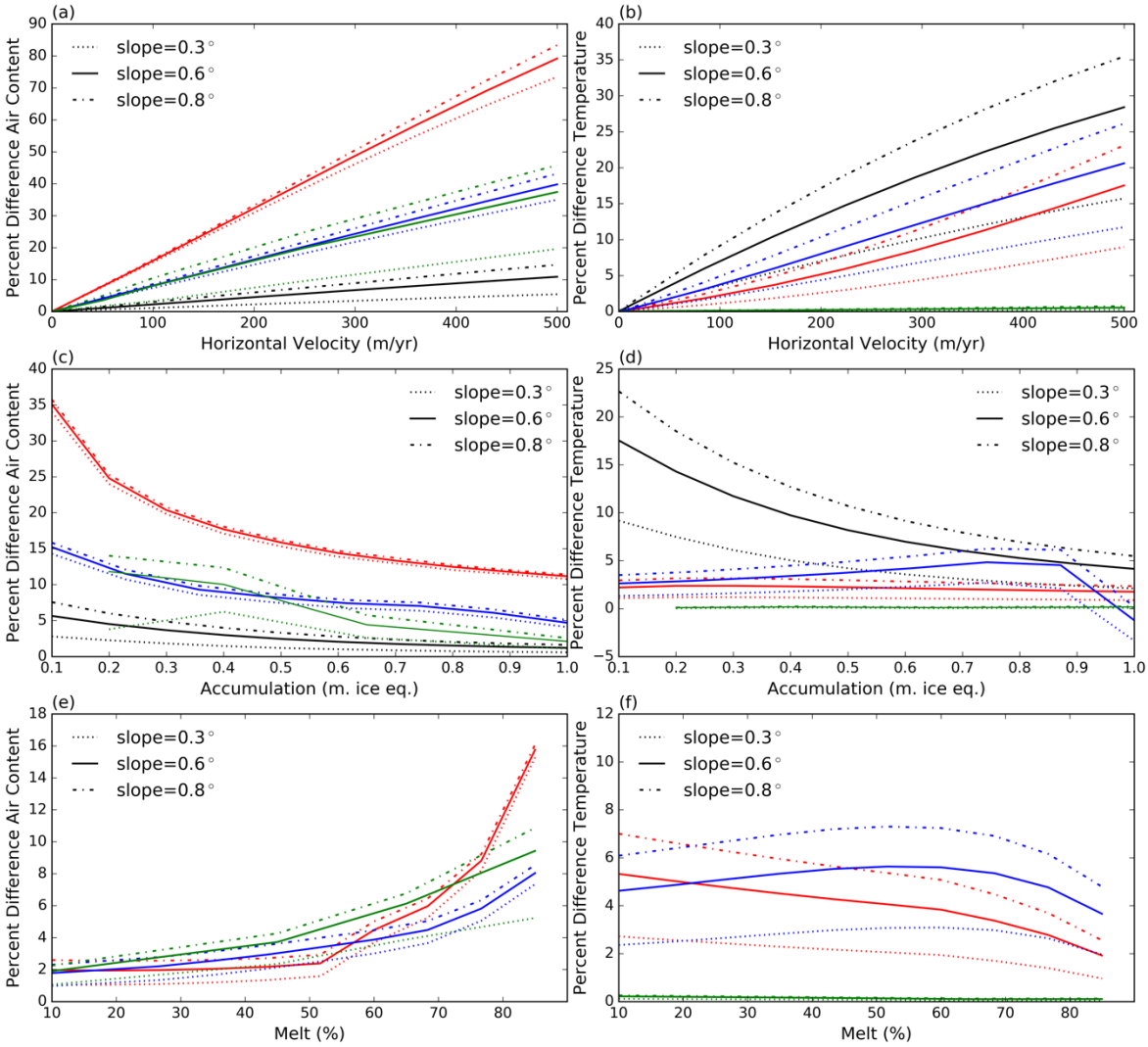

Figure 8. Modeled percent differences (2D-1D) for various climate scenarios found on the GrIS using several different models; dry model (black), Reeh model (red), tipping bucket model (blue), and continuum model (green). Left panels show percent difference in air content and right panels show percent difference in temperature. Positive percent difference in temperature represents colder temperatures. (a-b) represent various velocities, (c-d) represents various accumulation rates (ice equiv.), (e-f) represent different melt rates (ice equivalent).

3.2.3 Influence of Melt

Adding melt to the scenarios exacerbates the effects of advection on air content. In the velocity and accumulation simulations the dry scenario had the smallest increase in air content (Figure 8a; Figure 8c). The choice of melt scheme had a significant impact on the effects of

advection. The continuum model shows the least amount of increase in air content and the Reeh model shows the most.

The dry scheme resulted in colder temperatures at pore close off compared to the melt scenarios. The dry scenario has a pore close off approximately four times deeper than the melt scenarios. Increased depth of the pore close off leads to older firn at pore close, transported from higher on the ice sheet where it is colder.

Increasing the amount of surface melt exacerbates the affects of advection on air content. When surface melt is between 0-0.25 m ice equivalent, the influences of advection are minimal (Figure 8e). After 0.25 m ice equivalent the percent differences increases more rapidly, resulting in more air content in the 2D simulation. Increasing the melt from 0.25 to 0.42 m ice equivalent increases the affects of advection on air content by approximately 13%, 5%, and 5% for Reeh, tipping bucket, and continuum models respectively.

Each melt scenario displayed a different effect of advection on the temperature at pore close off (Figure 8f). The continuum model shows minimal differences in temperature at pore close off. In the Reeh model the temperature at pore close off decreases from ~5.5% (representing colder temperatures than the 1D at pore close off) with 0.05 m ice equivalent to ~2% colder at 0.43 m ice equivalent. Contrary to the Reeh model, the tipping bucket method is ~4.5% colder at 0.05 m ice equivalent, this increases to ~5.5% colder at ~0.28 m ice equivalent and then decreased to ~4% colder at 0.43 m ice equivalent. In this case, the difference between the 1D and 2D model increases between 0.05-0.28 m ice equivalent because latent heat is released closer to the pore close off. However, as melt increases the pore close off is shallower, which explains the decrease we see at 0.43 m ice equivalent.

3.2.4 Influence of Surface Slope

Steeper topography yields larger spatial gradients in melt, temperature, and accumulation; which are the driving factors for firn densification. Doubling the slope has little affect at smaller velocities but at larger velocities it can increase the affect advection has on air content by 4%-8% (Figure 8a). It is important to note that even with fast velocities a slope of 0˚ would have no effect from advection because there would be no spatial gradients of melt, temperature, and accumulation.

Increasing the surface topography has more influence on the temperature at pore close off than the total air content. Doubling the slope has the most affect when velocities are fast, yielding results that have more than 10% colder temperature at pore close off (Figure 8b). However, in the accumulation and melt tests, we observe ~2% decrease in temperature at pore close off when doubling the slope (Figure 8b; Figure 8d).

3.3 Greenland Transects

There are infinite combinations of velocity, accumulation, melt, and slope; we chose four different transects on the GrIS to look at combinations that are present on the ice sheet. The overall impacts of including advection in simulations of firn evolution along our four characteristic transects are summarized in Table 2.

3.3.1 EGIG Transect

By including 2D-advection, the firn density decreases by >50 kg m^{-3} for the EGIG transect resulting in increases in pore close off depth of 27 m, 8 m, and 4 m with the Reeh, tipping bucket, and continuum model respectively. Localized shallow topography, such as around 13-18 km, cause a decrease in the effects of 2D advection. (Figure 9a; Figure 10a; Figure

11a). An abrupt decrease in density can be seen from ~10-13 km where density is as much 30 kg m^{-3} less in the 2D simulation. This density decrease coincides with a 20 m yr^{-1} increase in velocity and an abrupt increase in the horizontal gradient of melt. In the lower 10 km we observe the largest decreases in density due to the increase in melt to 0.5 m ice equivalent and velocity to ~150 m yr^{-1}.

Advection makes the firn temperature measurably colder. Along the EGIG transect adding advection decreases firn temperature by ~1.5° C in the lower 15 km, 0.8°-1.0° C from 15-30 km, and <0.6° C above 30 km with the tipping bucket model (Figure 10a). The largest decrease in temperature is observed at ~7 km where firn is ~1.4° C colder with the 2D model using the tipping bucket model. Below 10 km on the transect, velocities reach >130 m yr^{-1} and melt exceeds 0.4 m ice equivalent and firn may have originated ~150 m higher on the ice sheet. The Reeh model simulations show temperatures decreasing ~0.8° C with the 2D model (Figure 9a) indicating that meltwater refreezing plays a key role in advection, since the temperature difference between the 1D and 2D models is small.

Air content along the EGIG transect increases by 1 m with advection, at the bottom of the transect, and decreases 0.2-0.6 m from 10-20 km with the tipping bucket method (Figure 12). The Reeh model simulation resulted in the highest increases in air content, reaching more than 2 m higher in the lower 10 km. The continuum model increased a maximum of ~0.5 m compared to the 1D model, staying relatively constant over the entire transect.

3.3.2 Jakobshavn Transect

We observe the largest density decreases below 10 km on the transect. Firn density decreases by >70 kg m^{-3} over the Jakobshavn transect, resulting in increases of pore close off depth of 50 m, 13 m, and 7 m with the Reeh, tipping bucket, and continuum model respectively

(Figure 9b; Figure 10b; Figure 11b). At ~10 km density is 30 kg m^{-3} lower in the tipping bucket and continuum model where velocity remains relatively high around 200 m yr^{-1}. We observe a sharp decrease between 0-3 km in pore close off using the Reeh model, while the tipping bucket and continuum models have a more gradual change in pore close off. Between 15-20 km the topography is shallower and subsequentially the gradient in melt decreases. In this range we see a localized decrease in the effects of 2D advection within the density profile. Contrarily, in the lower 3 km the slope sharply increases resulting in a localized increase in the effects of advection, demonstrating the importance of topography.

Firn temperatures decreased by as much as 3° C and 1.25° C with advection, in the tipping bucket and Reeh scheme respectively (Figure 9b; Figure 10b). The localized topography differences around 3 km is only seen in the tipping bucket scheme, where we observe sudden decreases in the effects of advection. The tipping bucket scheme also shows large decreases in temperature through the entire firn column while the Reeh scheme shows decreases only below 20 m depth in the firn column.

The firn air content increased with advection the most with the Reeh scheme and least with the continuum model. We observe an increase of air content of 3 m, 1.5 m, and 1 m at the bottom of the transect, with the Reeh, tipping bucket, and continuum model respectively (Figure 12). There is also a distinct decrease in the effects of advection between 15-20 km where the local topography is shallower.

Table 2. Summary of results from the four transects.

Transect	EGIG	Jakobshavn	K-transect	Helheim
Reeh model	~27 m change in pore close off Capacity is ~175% different at bottom of the transect, ~15% different at 10 km Below 10 km maximum temperature difference of 1º C	~50 m change in pore close off Capacity is 50%-200% different from 0-3 km Below 15 km maximum temperature difference of ~1.25º C	~14 m change in pore close off Capacity is ~200% different at bottom of the transect and declines to 5%-25% from 2-15 km Temperature differences negligible	~45 m change in pore close off Capacity is ~120% different at bottom of transect, above 2.5 km this decreases to less than 1% Below 2.5 km maximum temperature difference of ~2º C
Tipping bucket model	~ 8 m change in pore close off Capacity is ~50% different at bottom of the transect, 5-15% from 10-20 km Below 15 km maximum temperature difference of 1.5º C	~13 m change in pore close off Capacity reaches a maximum of ~200% difference and declines to 10% at ~10 km Below 15 km maximum temperature difference of more than 2º C	~3 m change in pore close off Capacity is ~33% different at bottom of the transect and declines to ~6% at 3 km Below 15 km maximum temperature difference of ~0.5º C	~19 m change in pore close off Capacity reaches a maximum of ~75% different, above 20 km this declines to less than 1% different Below 2.5 km temperature differences are greater than 3º C
Continuum model	~4 m change in pore close off Capacity is ~16% different at bottom of the transect, ~8% different at 10 km Temperature differences negligible	~7 m change in pore close off Capacity is ~45% different at bottom of transect and decreases to 14%-21% from 9-36 km Temperature differences negligible	~1.5 m change in pore close off Capacity is 3% different at bottom of transect and declines to less than 1% at 12 km Temperature differences negligible	~16 m change in pore close off Capacity reaches a maximum of 132% different and declines to 4% at 9 km Temperature differences negligible.

3.3.3 Helheim Transects

The effects of advection on the density structure along Helheim is only observed in the lower 2 km, where velocities and slope sharply increase (Figure 9c; Figure 10c; Figure 11c). Firn density decreases by >70 kg m^{-3} resulting in increases of pore close off depth of 45 m, 19 m, and 16 m with the Reeh, tipping bucket, and continuum model respectively. Above 10 km we observe minimal changes in the density. The velocity reaches speeds above 100 m yr^{-1}, however the shallow slope results in minimal horizontal gradients of melt and temperature.

Firn temperatures decreased up to 3° C and 2° C when including advection with the tipping bucket and Reeh models respectively (Figure 9c; Figure 10c). The effects of advection on temperature are observed higher on the transect than density effects. The temperature decreases above 1° C around 10 km in the tipping bucket model, and 5 km in the Reeh model. This temperature decrease happens below 10 m depth, contrarily decreases in temperature with advection are in the entire firn column in the tipping bucket model.

Increase in firn air content with 2D advection occurs below below 5 km (Figure 12). There is a 5 m, 2 m, and 2 m increase in air content with advection, for the Reeh, tipping bucket, and continuum model respectively. Above 5 km there is less than 0.5 m increase in air content under all simulations.

3.3.4 K-transect

There is little change to density and temperature structure in K-transect (Figure 9d; Figure 10d; Figure 11d). This is due to low velocities and slopes, all but eliminating the impact of ice flow. Density decreases 30 kg m^{-3} in the tipping bucket and Reeh models. However, there are limited effects on air content along the K-transect (Figure 12).

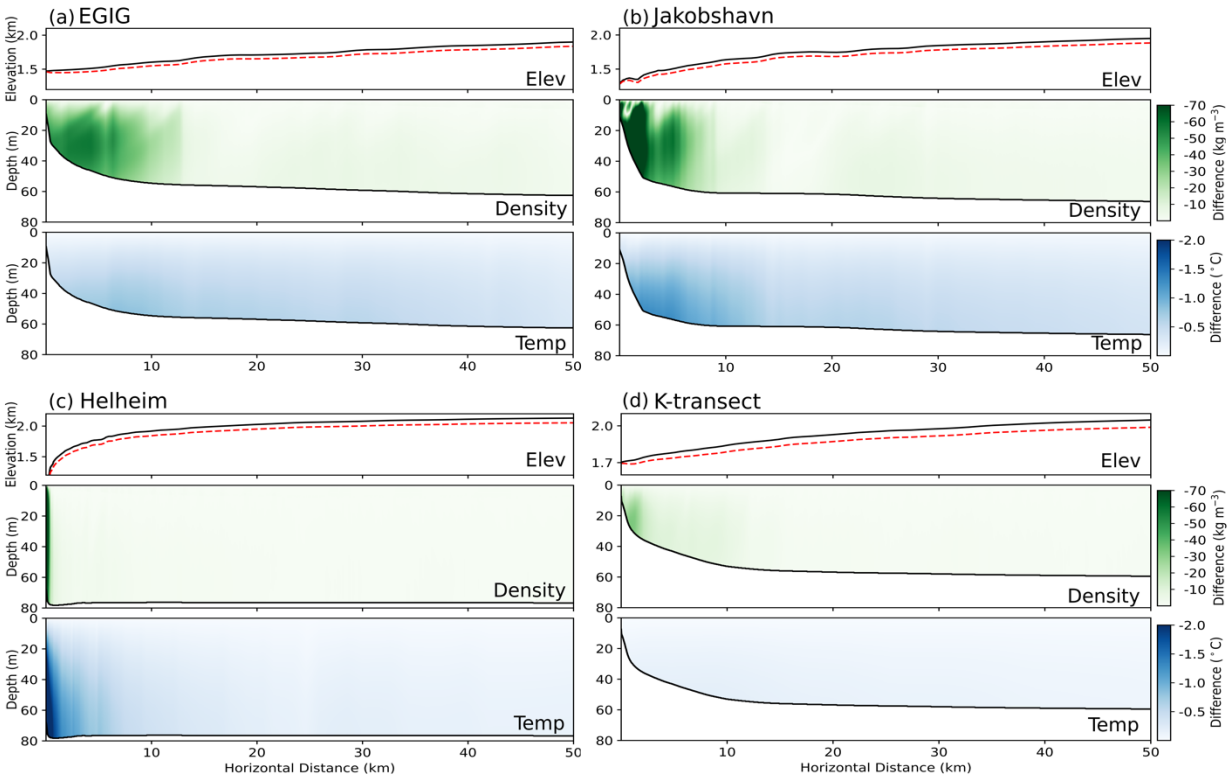

Figure 9. Modeled density and temperature differences using Reeh meltwater scheme (2D-1D) of a) EGIG b) Jakobshavn c) Helheim d) K-transect

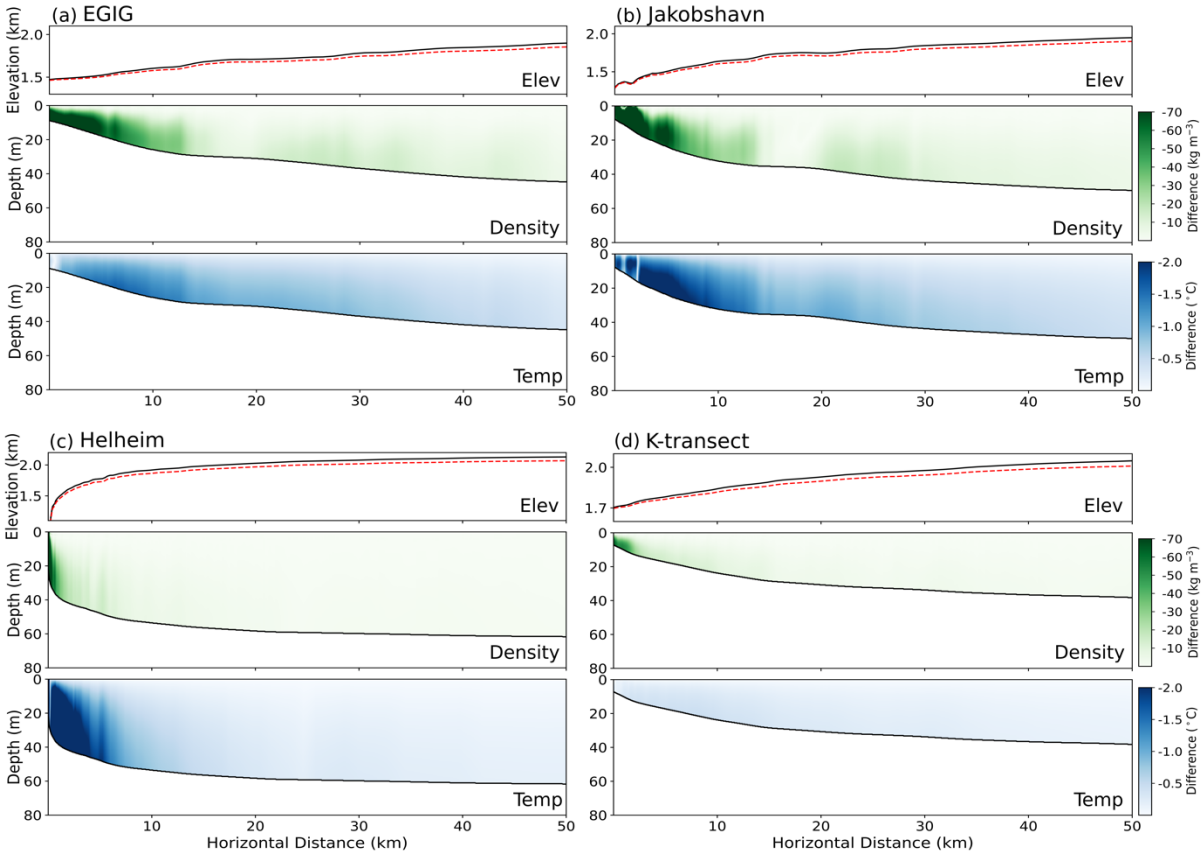

Figure 10. Modeled density and temperature differences using tipping bucket meltwater scheme (2D-1D) using a) EGIG b) Jakobshavn c) Helheim d) K-transect

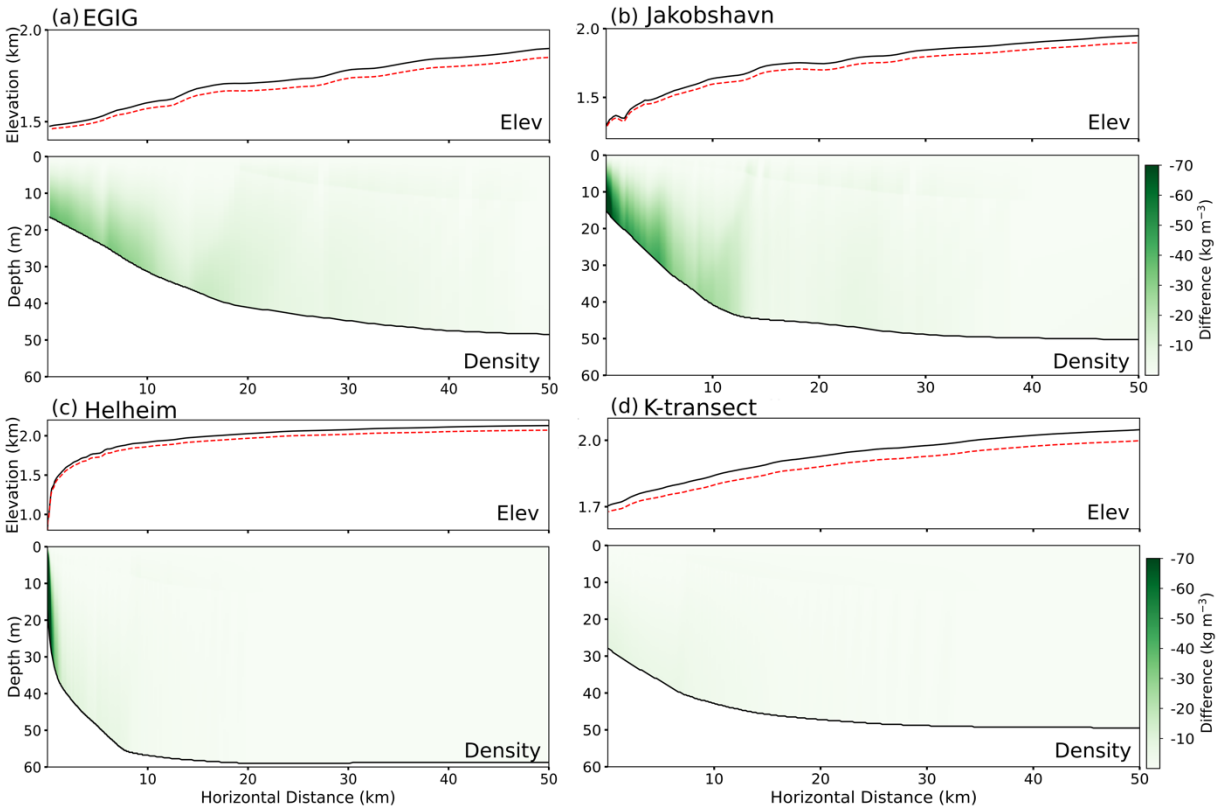

Figure 11. Modeled density differences using continuum meltwater scheme (2D-1D) of a) EGIG, b) Jakobshavn, c) Helheim, and d) K-transect

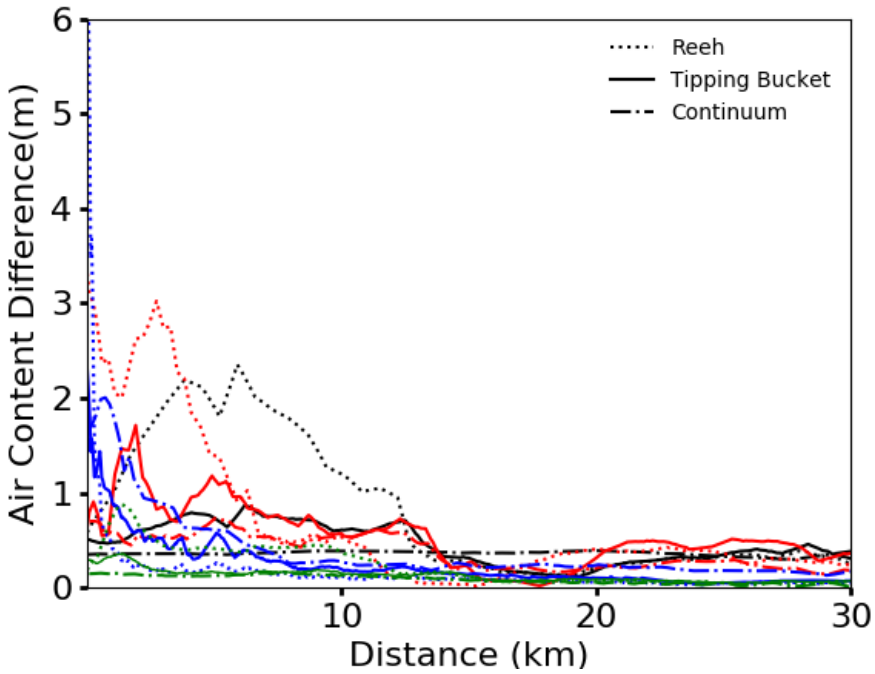

Figure 12. Modeled air content differences (2D-1D) for EGIG (black), Jakobshavn (red), Helheim (blue), and K-transect (green) with Reeh (dotted line), tipping bucket (solid line), and continuum (dashed line) models.

3.3.5 Comparison of Transects

We observe the most significant differences between the 1D and 2D model simulations along the lowermost 10-15 km of all percolation zone transects. Here, surface speed and surface slope increase substantially relative to the upper percolation zone, and overprinting from heavy melt is greatest. These effects were often abrupt; changes in pore close off and subsequentially air content in the lower 10 km tended to decrease suddenly in the lower 10 km. This is similar to what was observed in Figure 8e-f in the sensitivity results when melt was varied.

The choice of melt scheme also had a significant impact on the effect of advection. The Reeh scheme resulted in the largest increases in air content with 2D advection (Figure 12) while the continuum model resulted in the smallest decreases. However, the tipping bucket resulted in a larger decrease in density and increase in temperature compared to the Reeh model but pore close off was shallower resulting in less of an increase in air content. These uncertainties in melt penetration processes makes it difficult to quantify the effects of advection.

The degree of the effect of advection on air content varied for each transect due to the wide variety of atmospheric conditions. Jakobshavn and Helheim transects had the greatest air content differences. The K-transect had the least increase in air content, due to low velocities and shallow slopes. Lastly, the air content increases we observe are more affected by variance in ice content at depth and less to due with the advection of temperature.

3.4 Melt Feature Percentage

The 152 m long ice core collected at Crawford Point (Higgins, 2012) extends back to the year 1765 based on seasonal δO^{18} variations, and the modeled flow field using Reeh (2005) shows the bottom of the core originated ~260 years prior and about ~22 km up the flow line

(Figure 13). Thus, the flow model age estimate for the core-bottom is within 7-10% of the age determined by isotope methods.

Although MFP varies from year-to-year we are mainly interested in quantifying the long term trend of MFP with time and depth. The measured 152 m ice core time series shows a long term gradual change of ~0-25% and a 32 m drilled core (2018) shows a change of ~0-9% (Figure 14). The apparent change in MFP due to spatial gradients changes based on the firn depth. Figure 13 shows the change in MFP due to spatial gradients for 32 m, the modeled pore close off (60 m), the observed pore close (80 m), and the bottom of the core (152 m). The bottom of the core shows the maximum apparent change in MFP due to spatial gradients of ~7%. This represents firn being buried and transported along an ~20 km flow line and represents approximately a fourth of the measured signal at the bottom of the core.

We quantified the annual change in MFP per year in Figure 15. The MFP is changing over the entire firn column by 0.03% per year due to advection alone compared to the measured core value of 0.08% per year. The annual change in MFP will differ depending on the time frame of interest. Our modeling indicates that the depth (time) change in MFP that is attributable to advection alone, is inconsequential in firn generated in recent decades (i.e., <60 m depth). The shallower firn was deposited along the first ~5 km above Crawford Point, a region with very low slope and essentially no horizontal climate gradient caused by elevation. However, below ~60 m advection is altering the MFP by ~0.04% per year, where horizontal gradients increase sharply.

Assuming RACMO is a reasonable first-order estimate of climate this would imply that approximately an eighth to a fourth of the measured signal could be due to spatial gradients rather than temporal changes in climate in firn at deep depths. Therefore, even firn core records in the upper percolation zone, are a complex reflection of a spatial and temporally varying

climate. However, this effect is only exacerbated down-glacier where velocities and melt increase.

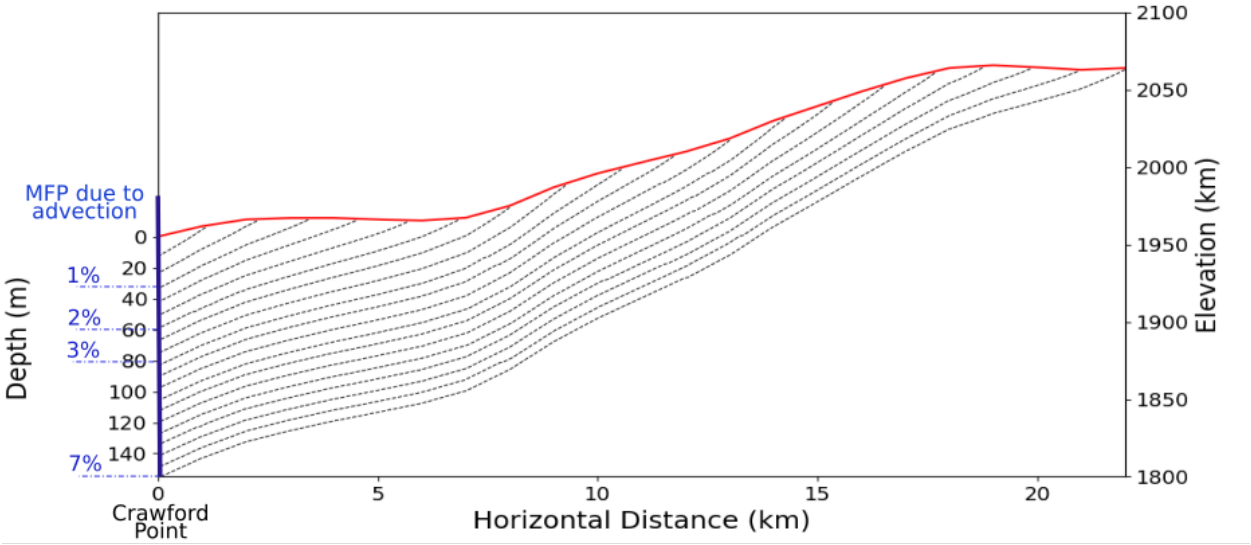

Figure 13. Modeled flow lines up ice sheet from Crawford Point. Depth (m) represents depth from the surface at Crawford Point and horizontal distance (km) represents distance up flow line from Crawford Point. Influence of advection (blue) on MFP is denoted at 32 m, 60 m (modeled pore close off), 80 m (measured pore close off), and 152 m (bottom of core).

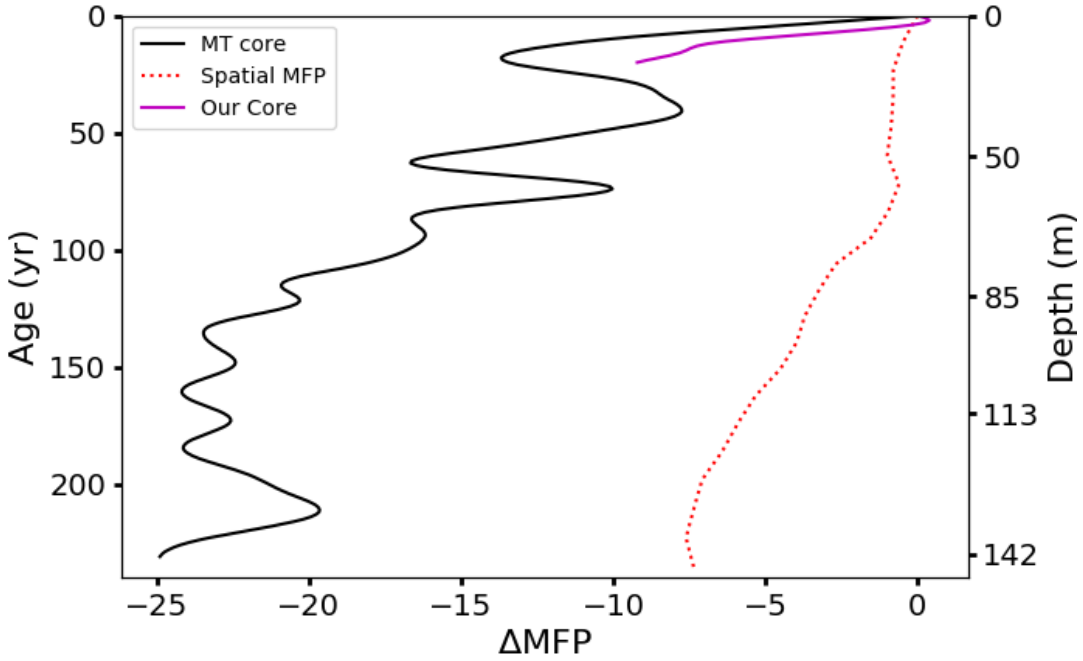

Figure 14. MT measured MFP compared to spatial MFP in depth and time. Age represents years before core was taken; MT core was taken in 2007 and our core was taken in 2018. Core goes to 142 m depth due to decadal averaging.

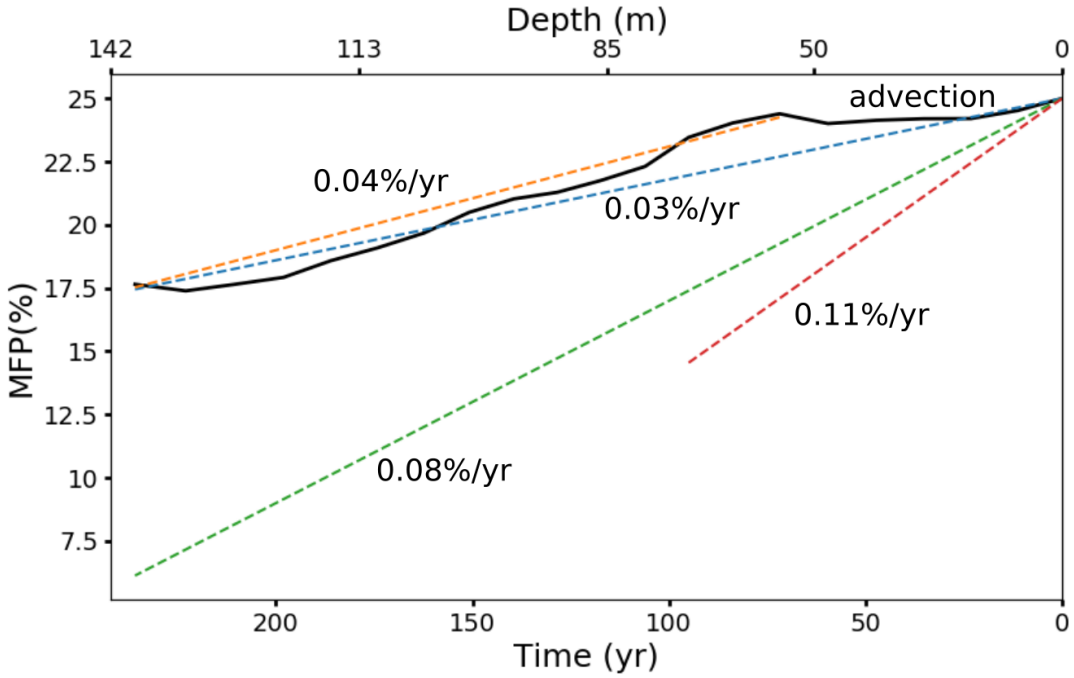

Figure 15. MFP versus depth in a core, measured and modeled. Black line is the apparent change in MFP generated by advection; time trends shown for full period (blue) and only firn older than ~70 years (orange). Time trends in MFP measured in an ice core and reported by Higgins (2012) shown for entire period (green) and since 1900-2007 (red).

4 Discussion

4.1 Processes influencing advection

The sensitivity tests demonstrate how low accumulation, high velocity, high melt, and steep topography favor preservation of deep pore space with 2D advection. Steep topography, which enhances spatial variance in the driving parameters (accumulation, velocity, melt, temperature), has the largest impact on the temperature solution especially when velocities are fast. For example, firn traveling 400 m yr^{-1} on a slope of 0.8˚ shows a 15% higher percent decrease of temperature at pore close off compared to a slope of 0.3˚. Low accumulation results in lower vertical velocities, leading to older firn at depth. Comparing a simulation ran with no melt, a 0.25 m ice equivalent accumulation compared to a 0.5 m ice equivalent accumulation resulted in firn at pore close off that was 45 years older under the lower accumulation. The firn under the lower accumulation scenario, originated higher on the ice sheet where conditions are colder and drier compared to firn under the high accumulation scenario. This principle is also observed under simulations with high velocities. Firn along the EGIG line traveling at ~140 m yr^{-1} actually originated ~200 m higher on the ice sheet where temperature and melt are approximately 0.9˚ C and 0.08 m water equivalent less.

4.2 Implications for Modeling Firn

4.2.1 Heterogeneity of the Percolation Zone

The range of conditions across the Greenland Ice Sheet vary in slope, velocity, and accumulation. At Helheim we see areas of high accumulation and velocity, at EGIG we see lower accumulation and moderate velocities, and Jakobshavn has moderate accumulation and high velocity (Joughin et al., 2010; Noël et al., 2018). In western Greenland slope changes are

quite gradual from the dry zone to ablation zone, in eastern Greenland by Helheim we observe sudden steep slopes more than 1º (Yi et al., 2005). The varied slope and conditions across the ice sheet demonstrate the heterogeneity of the percolation zone. Thus, one transect study should not be used to infer processes along other regions in the percolation zone.

In all transects the bottom of the percolation zone was the most affected by advection, while the top of the percolation zone was comparatively less impacted by horizontal motion. The bottom of the percolation zone is where we see the fastest velocities, largest melt, and in some cases the steepest topography, resulting in the largest change from 2D advection. The magnitude of the effect of advection varied across the ice sheet depending on the conditions in the area. For example, in Helheim the largest density decreases were only seen in the lower 2 km while at Jakobshavn we see large changes out to ~10 km.

4.2.2 Affect on Air Content

A suite of models have tried to quantify the air content of the upper 10 m, the entire firn column across the percolation zone, and even the entire ice sheet (Harper et al., 2012; Ligtenberg et al., 2018; Vandecrux et al., 2018). We find that in the lower areas of the percolation zone there is more pore space in 2D models compared to a standard 1D model; differences of more than 2 m of air content (Figure 12). One of the biggest uncertainties in our modeling experiment is the possible impact of heterogeneous meltwater infiltration on air content and how much meltwater can infiltrate into the excess pore space 2D advection creates in the lower percolation zone. Therefore, heterogeneous deep meltwater infiltration in the percolation zone is an important unsolved problem with even greater importance when 2D advection is accounted for when quantifying the firn air content.

4.2.3 Influence of Melt

Comparing the dry model run to the meltwater schemes in the sensitivity simulations, melt and the role of refreezing densification is the dominant process in 2D advection when comparing air content differences. In a dry simulation experiment a ~1º change in temperature corresponded to a density increase of only 1%. When adding in refreezing densification, the increase in density of each firn layer is controlled by the fraction of the layer that is refrozen meltwater and the release of latent heat. In the 1D model, it is assumed the entire firn column experienced the same amount of melt. The model with 2D advection takes into account that the firn at depth experienced a significant less amount of melt. For example, when running a Reeh model simulation a 5% increase in the amount of refrozen meltwater in a firn layer can cause the firn density in the annual layer to increase by ~10-19%.

The amount of latent heat released in the 2D model compared to the 1D model varies based on the amount of melt and the temperature of the firn. The increase in densification from latent heat is a function of how much ΔT it takes to cool the firn to the freezing point 0º C (Braithwaite et al., 1994). Therefore, with the 2D advection model we see a larger increase in densification due to latent heat warming because the firn at depth is colder. Therefore, more energy is released from latent heat using the 2D model.

We observe the largest decreases in temperature approximately 1-8 km above the ELA. At the ELA, the overall temperature difference between the 1D and 2D model is relatively small, despite fast velocities and steep slopes. This is due to the depth of pore close off decreasing towards the ELA. Shallower and younger firn at pore close off means there is smaller spatial gradients in climatic conditions.

The affect melt has on densification is related to the critical density in the densification function (550 kg m^{-3}). Past the critical density the rate of densification decreases (Herron & Langway, 1980). With increasing melt the uppermost firn layers will reach the critical density faster. This causes decreased densification resulting in an increase of older firn layers originating from higher on the ice sheet. Therefore, when the surface layer has enough refrozen meltwater to reach the critical density, we observe larger decreases in density when including advection.

4.2.3.1 Uncertainties

Modeling meltwater infiltration into firn is a complex process that has not been accurately captured by any model. This process has been considered in transient and steady state models (Ligtenberg et al., 2011; Reeh et al., 2005; Simonsen et al., 2013; Steger et al., 2017) but only in a 1D framework, and only with large simplifications of the infiltration physics. No prior work has accurately modeled the presence of piping events which can cause deep meltwater infiltration. This is difficult to model since meltwater infiltrates as an inhomogeneous process, traveling both horizontally and vertically (Pfeffer et al., 1991), therefore a 2D framework is needed. The depth meltwater is allowed to penetrate is quite important. Even small fractions of melt that make it past the annual layer can cause large differences on the deep firn structure based on where ice layers form.

The choice of meltwater infiltration scheme has a large impact on the effect of 2D advection and is a key uncertainty when we try to quantify our results. The Reeh scheme is oversimplified and incorrect but produces the largest impact of 2D advection. This is because there is no deep meltwater infiltration or overprinting at depth. The continuum model uses the most complex physics but has large uncertainties in the values chosen for permeability coefficients and grain sizes. The tipping bucket model simplifies the problem because it ignores

the complex physics governing the flow of water through it's own solid matrix. It simplifies the problem to use only density and cold content and assumes that the flow of meltwater is instantaneous. Knowing the uncertainties in the Reeh and tipping bucket model makes it easier to quantify the inaccuracies produced by model.

4.3 Evolution under changing climate

4.3.1 Past Climate

Several model studies have attempted climate reconstructions of the GrIS before the satellite era (e.g. Fettweis et al., 2017; Hanna et al., 2011). An increase in temperature was observed 1920-1930 on coastal weather stations (Chylek et al., 2006). After 1930 temperatures and subsequently melt declined until ~1970s (Chylek et al., 2006; Fettweis et al., 2017). Passive microwave satellite data has indicated that there was an increase in melt extent between 1979 and 1991 of 4.4% per year (Abdalati & Steffen, 1997). The total mass balance has been considered to be stable from 1961-1990 (Rignot & Kanagaratnam, 2006). However, a significant decrease in surface mass balance has been observed since the end of the 1990s when surface melt and temperature started increasing significantly (Fettweis et al., 2017). Since 1990 increasing temperatures have caused a ~3% increase per year in melt and runoff from 1990-2007 (Ettema et al., 2009). Increased melt has occurred everywhere on the ice sheet and modeled 1961-1990 average melt minus average 1991-2015 melt show a ~50-250 kg m^{-3} per year increase in the percolation zone (Van Den Broeke et al., 2016).

Since it was colder in the past, the deeper and older firn can be expected to be colder and dryer than the firn near the surface. Therefore, the shallow firn is even more different than the firn at depth. The recent increase in melt extent would have likely exacerbated the effects of advection compared to prior years where temperatures and melt were decreasing. The sensitivity

tests demonstrate how dry firn densification rates are secondary relative to the role of refreezing densification, thus exacerbating the role of advection. With a stable surface mass balance that was observed in the past, runoff likely did not occur abundantly in the percolation zone. We observed in the sensitivity tests that cases where there is runoff actually result in higher temperatures than the 1D case (Figure 8d). However, field results show the runoff likely occurs in the bottom 20 km of the percolation zone (Humphrey et al., 2012).

Although velocities have been increasing in Jakobshavn and Helheim towards the terminus of the glacier (Joughin et al., 2010) the interior of the ice sheet has been decelerating (MacGregor et al., 2016). One cause of the deceleration in the interior is due to the stiffening of the ice sheet over the past 9,000 years. This demonstrates how the ice sheet continues to respond to changing boundary conditions for thousands of years. In these areas the effects of advection would have been larger compared to present day according to the sensitivity tests where slower velocities reduce the influence of advection.

4.3.2 Future Climate

Past research (Meehl et al., 2012) calculates that global surface temperature could rise anywhere from 0.85-3.53ºC by the end of the century. This will be larger in the arctic as climate change is expected to be amplified in the polar regions (Meehl et al., 2012). With a warmer climate the ELA will shift to higher altitudes (Vizcaino et al., 2015), demonstrated by comparing surface mass balance between 1961-1990 and 1991-2015 (Van Den Broeke et al., 2016). In the simulations we observe that there may be remnant pore space beyond the ELA, as the ELA shifts to higher altitudes this remnant pore space may become even more important in regards to buffering sea level rise.

The affect advection will have with a changing climate is largely controlled by how heterogeneous the spatial changes occur. Currently, snowfall remains relatively stable as you move down the percolation zone for each transect. Melt tends to increase sharply towards the bottom of the percolation zone for each transect, where we see the largest decreases in density from 2D advection (Figures 9-11). Climate model simulations predict in the higher altitudes snowfall is expected to increase by ~0.1-0.2 m water equivalent per year while at lower elevations meltwater and runoff is expected to increase at a magnitude of ~1.0-3.0 m water equivalent per year by the end of the century (Fettweis et al., 2013). Increasing snowfall at the top of the percolation zone and increasing melt at the bottom of the percolation zone creates a larger spatial gradient in melt to accumulation than present. This increase will likely exacerbate the effects of advection, creating more spatial differences in melt and accumulation. Increased accumulation at higher latitudes and decreased melt at lower altitudes may also cause steeper topography going from the dry zone to the ablation zone; steeper topography increases the affects of advection.

It is difficult to predict how increased melt in the future will affect Greenland velocities. It has been suggested that increased velocities can be caused by increased melt and basal lubrication of the bed (Zwally et al., 2011). However, observations show that the basal water system adjusts quickly to increase amounts of meltwater (Van De Wal et al., 2008). In addition, this would only affect the lower percolation zone where runoff occurs, assuming meltwater reaches the base of the glacier.

Increasing the amount of precipitation that falls as rain may also have an impact on the role of advection. Snowfall will increase during the winter months but during summer months higher temperatures will result in an increase in rainfall from present day climate in a century

(Fettweis et al., 2013). Increased rainfall may cause the upper firn layers to reach the critical density faster. The sensitivity tests (Figure 8e-f) show how the influence of advection increases when this happens, decreasing the rate of densification.

Projections on refreezing capacity depend how deep meltwater can infiltrate. Our experiments show how advection creates more deep pore space (Figure 12) but if meltwater can not infiltrate into deep firn then the extra pore space will not provide a buffer to sea level rise. The refreezing capacity on the ice sheet has a direct control on how long the SMB will stay positive. If climate model scenarios ran with refreezing capacity constant SMB would stay positive for several decades longer (Angelen et al., 2013). Model scenarios indicate that a 10-year running average of GrIS SMB will turn negative in several decades and cause a 24% decrease in refreezing capacity in less than century (Angelen et al., 2013).

4.4 Implications for Ice Core Interpretation

Understanding how the amount of surface melt on the GrIS has changed temporally is important for surface mass balance prediction models. In the percolation zone it is estimated that about 40-50% of the meltwater may never actually escape (Janssens & Huybrechts, 2000). Several studies have been conducted examining firn cores in the percolation zone in order to quantify how surface melt has changed temporally. By comparing annual accumulation to the refrozen meltwater in firn layers studies can then calculate the annual Melt Feature Percentage (MFP). Studies can infer how melt has changed over the past and if the increase in melt we are seeing now is unprecedented of the past.

Many studies assume that firn at depth originated at the surface, when the firn actually originated higher on the ice sheet where there is less melt and colder temperatures. This

assumption could mean that results of how surface melt has changed in the past could be skewed by spatial gradients. Less melt at depth may actually be due to firn originating up flow on the ice sheet where there is less melt. Higher on the ice sheet this becomes less important. Close to the ice divide velocities are lower and slopes tend to be less steep with less melt. The sensitivity tests (Figure 8) show how these conditions decrease the importance of advection.

We analyzed Crawford Point as a case study in order to investigate how ice flow may influence deep core interpretations. The flow lines in Figure 13 represent the path deep firn follows and demonstrates how firn can originate over 20 km higher on the ice sheet where it is ~1° colder and 0.04 m water equivalent less in melt. Shallow depths around a few decades old or ~30 m deep show very little change in MFP due to advection (Figure 13; Figure 14). This is expected since spatial changes in climatic conditions are small over shorter time scales and this is amplified by shallow slopes within 10 km of Crawford Point. Measured MFP is also likely to be amplified over shorter time intervals, yielding a higher slope with regression tests.

Over long century-scale time periods (1765-2007) the measured Crawford Point MFP increases by ~0.07-0.08% per year (Higgins, 2012). However, melt events prior to 1900 were minor and infrequent resulting in a more recent trend from 1900-2007 with an increase of 0.11% per year (Figure 15). Fitting a trend to spatial MFP yields a change on the order of ~0.03% per year; approximately a third of the measured signal measured at the core. Therefore, ice cores from the percolation zone can have a spatial component that must be evaluated and it is not justifiable to ignore the influence of ice flow when interpreting deep cores.

Understanding the effect of spatial gradients can help quantify research such as how melt intensity has changed (Trusel et al., 2018) or research correlating cores to determine how surface melt has changed in the past (Graeter et al., 2018). Even though these cores are drilled high in

the percolation zone Figure 15 shows how spatial gradients may be a significant portion of the MFP. The affect of advection on MFP largely depends on the location of core. Lower in the percolation zone this effect will only amplify because climate gradients and velocity increase.

The Crawford Point is one example of how ice flow can influence a deep core interpretation. However, this will change with the location on the ice sheet and the percolation zone. In order to quantify the effect spatial gradients have on firn cores in the percolation zone, we analytically derived an equation assuming melt, accumulation, and velocity are known up flow line and have remained relatively unchanged.

$$\frac{dMFP}{dt}\,(\mathrm{v},\mathrm{x}) = \frac{MFP\big(x(t_f)\big) - MFP(x(t_0))}{t_f - t_0} \tag{17}$$

Where *MFP(x)* is calculated as

$$MFP(x) = \frac{m(x)}{b(x)} \tag{18}$$

where *b* and *m* are the accumulation and melt at distance *x* up-glacier. We then need to solve $x(t_f)$ and $x(t_0)$, $x(t_f)$ is the distance away from the core at the final time of interest and $x(t_0)$ is the distance away from the core at the begin time of interest. This will be at 0 m and 0 years if analyzing from the surface of the core at present time. In order to solve for $x(t_f)$ the variable velocity field must be taken into account by solving the following ODE for $x(t_f)$ and $x(t_0)$,

$$x(t) = -\int_{t_0}^{t} v(x)dt \tag{19}$$

Equation 17 can be used to determine trends in the spatial MFP and then Equations 18-19 can be combined to generate a time series of MFP recording the spatially varying climate advected by

ice flow. The uncertainty with velocities can be large and is calculated assuming shallow ice velocities.

5 Conclusions

Our model simulations show how ice flow can influence the density and thermal structure of the percolation zone in several different ways. Areas in the percolation zone that are characterized by fast velocities and steep slopes will have the most effect from ice flow. However, the percolation zone is very heterogeneous and the effects of advection can vary. We observed the lowest 10 km in the percolation zone from the Jakobshavn transect showing the most influence from 2D advection, changing air content by 10s of percent, while the K-transect showed the least amount of changes.

This research has implications for future studies analyzing melt features in ice cores in the percolation zone. Even higher up in the percolation zone, where firn density and temperature are relatively unaffected by ice flow, the spatial signal could account for a fourth of the observed MFP changes. That number increases down flow in the percolation zone. We provide an analytically derived equation that can be used to calculate the approximate effects of spatial gradients on an ice core. However, this assumes spatial gradients are unchanged and more work is needed in order to determine the complex temporal and spatial gradients in the firn.

6 Appendix A: Firn Model Comparison

6.1 FirnMICE

An analysis was completed to compare multiple firn models with the FirnMICE experiment (Lundin et al., 2017). The models tested were HL transient (Herron & Langway,

1980), Arthern (Arthern et al., 2010), Ligtenberg (Ligtenberg et al., 2011), and Zwally & Li (Li & Zwally, 2004) (not utilized in FirnMICE).

The FirnMICE experiments tested several dry firn models against each other using various temperatures and accumulations. The models were spun up 10,000 years with steady state conditions. Six experiments were ran, three had constant accumulation and three had constant temperature. After 100 years a time step change in accumulation or temperature would occur. Figure S1 shows the conditions that were applied for each experiment.

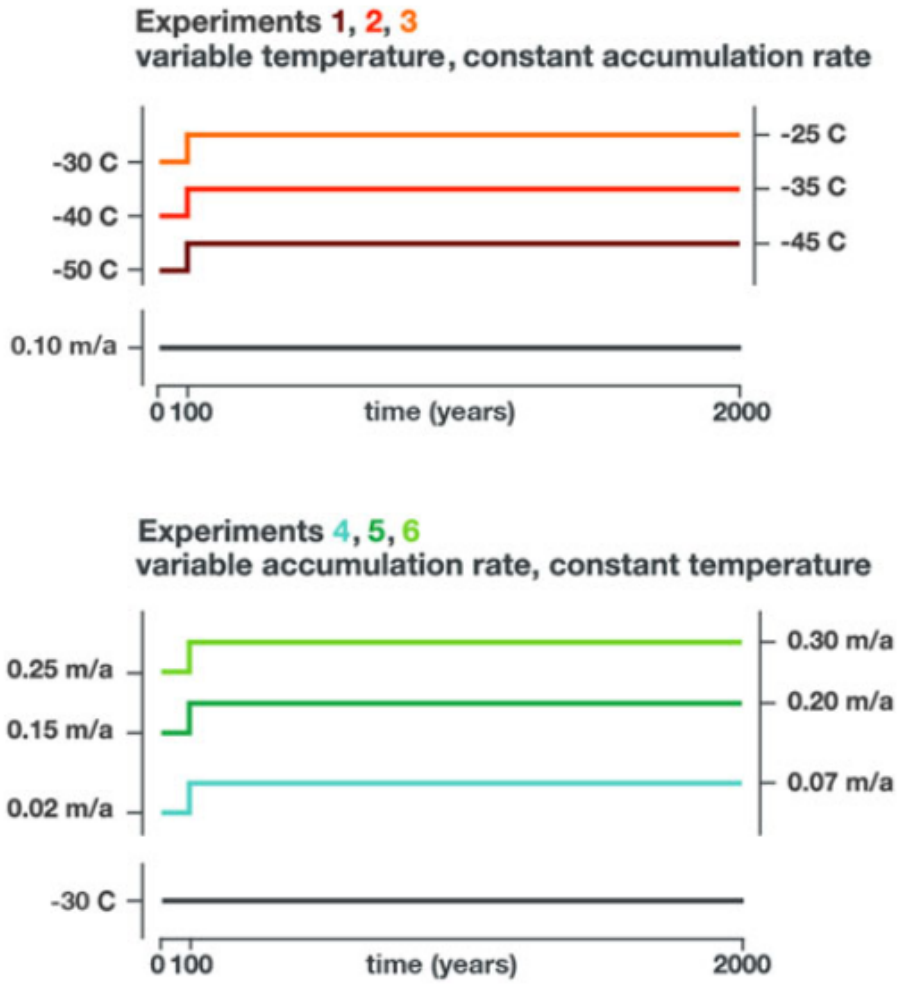

Figure S1. FirnMICE boundary conditions for six experiments. Models were spun-up for 10,000 years with steady state conditions. Adapted from Lundin et al., 2017.

We compared the HL, Arthern, Ligtenberg, and Zwally & Li models. HL, Arthern, and Ligtenberg describe the firn densification derivative different for densities above and below the critical density of 550 kg m^{-3} where the processes of firn densification alter. Zwally and Li define a single constant with an Arrhenius type relation. The Herron and Langway model was chosen due to simplicity and similar results compared to the other models tested.

6.1.1 Herron and Langway

Herron and Langway used depth-density data from 17 sites in Greenland and Antarctica with varying temperature and accumulation rates. They empirically fitted lines for each densification stage and calculated a rate constant for the first two stages of densification based on accumulation and temperature. Rate constants were fitted by a least-squares method to the field data. The total densification process can then be defined using the material derivative.

$$\frac{D\rho(t,z)}{Dt} = \frac{\partial \rho}{\partial t} + \omega \frac{\partial \rho}{\partial z} \tag{19}$$

Results from the FIRNmice are shown in Figure S2-S3. Our transient HL model matches up well with the other models used.

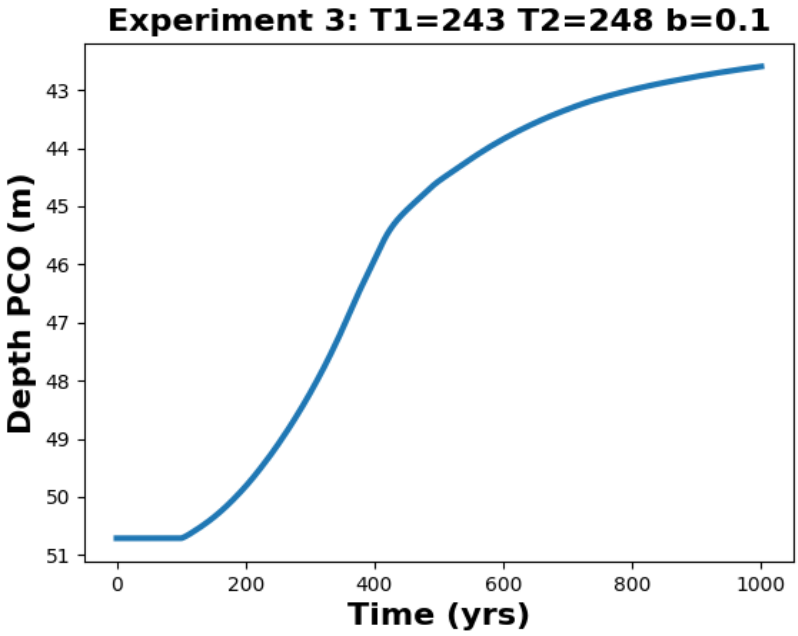

Figure S2. HL transient model depth at pore close for FirnMICE experiment 3.

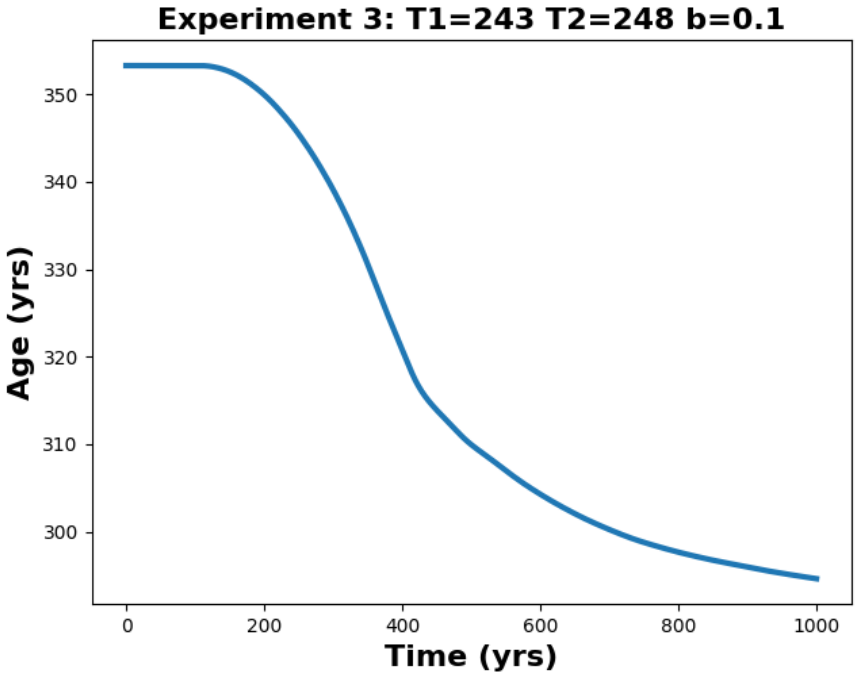

Figure S3. HL transient model age at pore close for FirnMICE experiment 3.

6.1.2 Arthern and others (2010)

Arthern coupled densification, heat-transfer, and grain-growth and used the basic Herron and Langway model formulation and is derived from a sintering theory. They derived activation energy by trial-and-error comparison with a time series of compaction rates.

$$\begin{cases} c_0 = 0.07bgexp\left(\frac{-E_c}{RT} + \frac{E_g}{RT_{av}}\right) \text{if} \rho \leq \rho_c \\ c_1 = 0.03bgexp\left(\frac{-E_c}{RT} + \frac{E_g}{RT_{av}}\right) \text{if} \rho_c < \rho \end{cases} \quad (20)$$

Where b is the mass accumulation rate (kg m^{-2} yr^{-1}), g is gravitational acceleration, E_c is 60 kJ/mol and E_g is 42.4 kJ/mol.

The Arthern model was decided not to be used due to the models lack of response to accumulation rates. This was found in our experiments and concluded in FirnMICE. The models insensitivity to accumulation is because the physics are based on Nabarro-Herring creep, where there is a linear stress and grain size dependence reducing the sensitivity to the accumulation rate.

6.1.3 Ligtenberg and others (2011)

Ligtenberg updated Arthern's model empirically using 48 ice cores in Antarctica. The formulation becomes more accumulation dependent based on -ln(b).

$$\begin{aligned} c_0^{(LIG)} &= M_0 c_0^{(ART)} \\ c_1^{(LIG)} &= M_1 c_1^{(ART)} \end{aligned} \quad (21)$$

$$\begin{cases} M_0 = 2.366 - 0.293ln(b) \text{ if } \rho \leq \rho_c \\ M_1 = 1.435 - 0.151ln(b) \text{ if } \rho_c < \rho \end{cases} \quad (22)$$

Where b is the mass accumulation rate (kg $m^{-2}yr^{-1}$).

6.1.4 Zwally & Li

Zwally and Li constructed a firn model based on field and laboratory experiments for grain growth and ice creep. Unlike HL, Arthern, and Ligtenberg they use a single rate constant for both stages of densification. They used data from grain growth to find the best-fit curve for activation energy. One of the main uncertainties in their model is the empirical normalization factor (beta) they used to account for differences between rates for densification and grain growth making the model data dependent. Beta is usually a number between 2 and 8. The Zwally & Li model is driven by temperature and includes updates to account for vapor transport theory.

7. Appendix B: Thesis in Manuscript Form

Abstract

One dimensional simulations of firn evolution neglect horizontal transport during burial. Using a suite of model runs, we quantify the impacts of advection on the development of firn density, temperature, and stratigraphy of melt features. The simulations isolate processes in synthetic runs and investigate an ice core site and four transects of Greenland's percolation zone. We find that horizontal ice flow interacts with topography, climate gradients, and meltwater infiltration to influence the evolution of firn column structure. The advection process tends to increase the pore close-off depth, reduce the heat content, and decrease the frequency of melt features with depth, by emplacing firn sourced from higher locations under increasingly warm and melt-affected surface conditions. Pore close-off and temperature are mainly impacted in the lowermost 20 km

of the percolation zone, but ice flow can introduce substantial change in melt feature stratigraphy across the percolation zone.

7.1 Introduction

Summer melting of bare ice, epitomized by stream networks and moulins, represents a relatively small portion of the Greenland Ice Sheet (GrIS) periphery since about 90% of the ice sheet's area is perennially snow covered accumulation zone (e.g., Ettema et al., 2009). A large fraction of the snow covered region also experiences melt (Figure 5a): between 50-80% melted during summers of the period 1958-2009 (Fettweis et al., 2011), for example. Further, the inland extent and duration of melting have demonstrated increasing trends and frequently established new records (Mote, 2007; Tedesco, 2007; Tedesco 2013). Melting accumulation zone (ie. the percolation zone) is therefore an increasingly important aspect of the ice sheet, and so too are the glaciological processes governing the snow/firn interactions with surface climate.

Meltwater from the lower accumulation zone may run off from its point of origin (e.g. Machguth et al., 2016), while at higher elevations the water may simply infiltrate into cold snow and firn to fill underlying pore space, forming ice when it refreezes (e.g., Braithwaite et al., 1994; Harper et al., 2012) or remaining liquid if it does not (e.g., Forster et al., 2014; Humphrey et al., 2012). While current model fidelity prevents confident constraint on the amount of melt retained in the percolation zone, existing estimates are that 40-50% of the meltwater generated never escapes (Angelen et al., 2013; Janssens & Huybrechts, 2000; Reijmer et al., 2012). The firn layer of the GrIS percolation zone is thus a potential reservoir for storing surface meltwater and latent heat (Harper et al., 2012; Pfeffer et al., 1991). Still unclear, however, are the evolutionary processes governing firn structure and ability to accommodate meltwater.

The percolation zone is a region with relatively high horizontal motion compared to submergence rate (cf. divide regions) (Figure 5b). Ice sheet flow displaces the firn column to lower elevation, where it is buried by subsequent winter layers experiencing higher intensity summer melt. Thus, the deep firn column's structural makeup and thermal state results from a climate that varies in both time *and* space. The impact of this effect is undocumented, and likely varies substantially around the ice sheet. This adds to the uncertainty regarding the structural framework of the firn column, the amount of deep pore space that could absorb future meltwater and heat, and the interpretation of melt feature stratigraphy within ice cores collected from these regions.

Here we investigate the role that horizontal ice motion plays in driving the structural evolution of the deep firn layer. We utilize previous approaches for modeling firn densification and meltwater infiltration, but extended the analysis to two dimensions to include advection of the domain due to ice flow. Our investigation is focused on synthetic modeling of isolated processes, four differing transects of the GrIS percolation zone, and partitioning the signal of climate change from an advection signal within ice cores from the percolation zone.

7.2 Methods

7.2.1 Model Description

The density and thermal structure of firn within the percolation zone is a function of temperature, accumulation rate, and melt/refreezing processes (e.g. Herron & Langway, 1980; Reeh et al., 2005). The spatial gradients in these parameters, coupled with the speed at which the ice moves through the gradients, determines the influence of ice flow on deep firn structure. We simulate

these processes using a transient, thermo-mechanically coupled model for firn densification and heat transfer that includes meltwater penetration and refreezing (see Section 2.1).

Changing surface conditions as ice flow transports the firn column down-glacier are translated to time-varying boundary conditions using surface speed. This approach captures the processes of burial, ice layer formation, and vertical heat transport, and is advantageous in that it easily accommodates a range of meltwater infiltration schemes (detailed below). It does, however, lack horizontal heat diffusion. Testing against an explicit 2D model for densification and heat transport including horizontal diffusion yielded negligibly different results (Figure 7, section 3.1). Omission of this process therefore has little effect on model results.

Firn temperature is modeled by solving the standard one-dimensional time-dependent heat-transfer equation with latent heat from the refreezing of meltwater (Paterson, 1994). We implement the time dependent model for densification from Herron and Langway, (1980), based upon it's relatively simplistic formulation with few tuning parameters and favorable comparison with other densification schemes (Lundin et al., 2017). Temperature, density, and vertical velocity were coupled together and solved using the finite element library FeniCS with Galerkin's method and an explicit time step. We use a Lagrangian domain, with a moving grid and constant boundary positions with time. Dirichlet boundaries for state variables temperature, density, and vertical velocity (based on accumulation rate) are imposed at the model surface, and vertical gradients in these variables are set to 0 at the model base. Detailed description of the model setup is presented in Section 2.1.

Modeling complex and heterogeneous meltwater infiltration in firn remains an outstanding problem of critical importance and solving this is beyond the scope of this project. Instead, our approach is to implement three existing infiltration schemes which vary in complexity and reflect a range of approximations. The first model considers only shallow infiltration, assuming that all meltwater refreezes in the top annual layer (Reeh et al., 2005). The second implements a standard tipping bucket method (Ligtenberg et al., 2018; Munneke et al., 2014), allowing meltwater infiltration as far as permitted by thresholds for cold content and irreducible water content. Meltwater percolates until reaching a firn layer with a smaller irreducible water content than the available liquid water or the pore close off density is reached; any remaining meltwater runs off instantaneously. The third infiltration model implements a continuum approach (Meyer & Hewitt, 2017), simulating the physics of water flow based on Darcy's Law, and treating both saturated and unsaturated conditions.

7.2.2 Model Experiments

The influence of horizontal advection on firn structure at depth is dependent on ice flow speed and spatial gradients in climate forcings (temperature, melt, and accumulation). We conducted an initial test of model sensitivity to each of these variables to understand, in isolation, the influence of changes in these processes on firn structure. We then applied the model to four flowline transects across GrIS' percolation zone representing a spectrum of ice sheet and climate conditions.

7.2.2.1 Sensitivity Analysis

Synthetic sensitivity tests were performed around a base scenario with horizontal velocity of 100 m/yr and an accumulation rate of 0.5 m/yr water equivalent, approximately matching conditions along the EGIG transect. Horizontal velocities, accumulation rate, and total melt were then varied across ranges of values spanning the conditions that may occur in the GrIS percolation zone (see section 2.2.1). Additionally, we imposed three different surface temperature gradients in each simulation to determine model sensitivity to a spatially varying surface temperature boundary.

7.2.2.2 Greenland Transects

Our 2D modeling approach was implemented at four test transects spanning the GrIS (Figure 5): 1) the well-studied EGIG transect in western GrIS, 2) a transect feeding Jakobshavn Isbrae, 3) the K-transect in southwest GrIS, and 4) a transect extending into Helheim Glacier. These four study profiles were selected to capture a wide variety of ice sheet conditions (Table 1). Surface velocities along study transects were defined from satellite velocity data (Joughin et al., 2010), and 1980-2016 average climate variables were selected from RACMO2.3p2 (Noël et al., 2018). This time period roughly captures the increase in GrIS melt since the late 20th century (Fettweis et al., 2011). Two-dimensional simulations were performed over each transect, in addition to 1D simulations at 600-1700 locations, variably spaced based at annual displacements between profiles. The latter were used for baseline comparisons of the effects of including or not including advection of the firn column.

7.2.2.3 Ice Core Example

A commonly used metric for quantifying changing climate conditions from firn cores is the annual increment of surface melt, or Melt Feature Percent (MFP) (Koerner, 1977; Kameda et al., 1995; Trusel et al., 2018). We examine the MFP signal at Crawford Point, located along the EGIG line transect to exemplify the roles of both advection and changing climate in trending MFP time series. This site is relatively high elevation in the percolation zone, with shallower surface slope, slower velocity, and far less surface melt than the lower percolation zone. In recent decades the average summer experiences about 15 days of melt (Mote, 2007). In 2007, a 152 m ice core was collected and the melt feature percent (MFP) was logged in an ice core with annual layers dated by isotope methods (Higgins, 2012).

We modeled the 2D firn evolution on a flow line leading to Crawford Point using datasets for the modern state. Ice surface geometry (Morlighem et al., 2017) and velocity (Joughin et al., 2010) datasets were used for converting from space to time; and, mean melt and snowfall values from RACMO2.3p2 (Noël et al., 2018) were used to determine spatial climate gradients. We assume the spatial gradients in these datasets have not changed over a century time scale. The validity of this assumption is unknown and perhaps tenuous; our intention, however, is a demonstration of the advection process constrained by ice sheet conditions. Furthermore, if there are in fact large time changes in gradients, this only adds complexity to advection signal. Finally, we employ the Reeh (2005) model for infiltration to be consistent with the assumption of shallow infiltration employed by MFP observational studies.

7.3 Results

7.3.1 Sensitivity Tests

Including horizontal advection in simulations yields greater air content in the firn column and therefore increased depth to pore close off than 1D results (Figure 8). The impact of advection is a function of accumulation, with smaller accumulations causing a 25-35% increase in the depth to pore close off in 2D simulations relative to the 1D model runs. This stems from reduced densification rate under smaller annual increments of overburden, and thus longer preservation of cold and porous firn that becomes deeply buried firn further down-glacier. Adding melt gradients to the scenarios exacerbates the effect, with wet surface conditions overprinting dryer conditions at depth.

Adding advection to simulations also decreases the firn temperature; the temperature profile and temperature at pore close off reflect advected firn from higher, colder conditions. Heat content is strongly influenced by choice of melt scheme: for example, under very high accumulation and melt, the tipping bucket method yields deep penetration of water and warmer firn temperature at depth (cf. the 1D case). Steeper topography yields larger along-flow gradients between melt, temperature, and accumulation, causing greater disparities between 2D-avection and 1D-profile simulations. The ice flow speed has potential to strongly impact simulations with 2D-advection, but importantly, this impact is highly dependent on surface gradients and melt infiltration. In simulations with high horizontal gradients in climate (ie. steep topography), and limited melt penetration (ie. infiltration following Reeh (2005)), model results including ice flow differ from 1D by up to four-fold at highest speeds.

7.3.2 Transects

The most significant differences between the 1D and 2D model simulations are along the lowermost 10-15 km of our four representative transects. Here, surface speed and slope (a proxy for climate gradients) both increase substantially relative to the upper percolation zone, and the surface experiences heavy melt. By including ice flow in these firn simulations, the density differs by >50 kg m^{-3} for the EGIG, Jakobshavn, and Helheim transects (Figure 9; Figure10; Figure 11), resulting in increases to pore close off depth of up to 8 m, 13 m, and 19 m, respectively. The commensurate impacts on total air content in the firn column can also be large: for example, along the EGIG transect it changes by ~50% in the lower 10 km, and by 5%-15% along the next 10-20 km.

The different melt infiltration schemes yield variable impacts on firn air content from advection. The largest impact is with Reeh (2005) scheme, under which the inclusion of advection in simulations increases the firn column air content by up to several meters from a 1D simulation (Figure 12). Local changes in surface slope along the transects both enhance and diminish the impacts of advection on the underlying firn structure, complicating the 2D firn geometry of the percolation zone. The changes to density structure throughout the K-transect are comparatively small because the topography and speeds are so much lower than most places on the ice sheet (Table 1), all but eliminating the impact of ice flow (Figure 10d).

The process of advection generates colder firn temperature profiles. Along the EGIG transect advection decreases firn temperatures at the depth to pore close off by 1.0°-1.5° C in the lower 15 km, and by 0.8°-1.0° C in the next 15 km. With the high speeds, steep topography, and heavy

melt of the lowermost reaches of Jakobshavn and Helheim transects, firn temperatures were altered by as much as 3° C by including advection.

7.3.3 Ice Core Example

The 152 m long ice core collected at Crawford Point (Higgins, 2012) extends back to the year 1765 based on seasonal del018 variations, and the modeled flow field shows the bottom of the core originated ~260 years prior and about ~22 km up the flow line (Figure 13). Thus, the flow model age estimate at the core-bottom is within 7% of the age determined by isotope methods.

Our modeling indicates that at Crawford Point, the depth (time) change in MFP that is attributable to advection alone is inconsequential in firn generated in recent decades (i.e., <60m depth). The shallower firn was deposited along the first ~5km above Crawford Point, a region with very low slope and essentially no horizontal climate gradient caused by elevation. Below this depth, there is an abrupt inflection to continuously decreasing MFP to the bottom of the core (Figure 15). At depths >60 m, the change in MFP due to advection amounts to about 0.04% per year.

7.4 Discussion

7.4.1 Uncertainty due to Infiltration

The choice of meltwater infiltration scheme has a large effect on the simulated impacts of firn advection in the percolation zone and is a key uncertainty in the robustness of our results. In reality, water moves vertically as a wetting front propagating downward from the surface (Colbeck, 1975) and importantly, also by complex and unpredictable inhomogeneous infiltration

processes (Marsh & Woo, 1984; Pfeffer & Humphrey, 1996). With so little known about deep infiltration, none of our schemes are likely to be entirely accurate: the Reeh (2005) scheme only allows melt penetration within the annual snow increment which is known to be incorrect, especially low in the percolation zone where melt rates are high (e.g., Humphrey et al., 2012); the continuum model (Meyer & Hewitt, 2017) uses the most complex physics, but has large uncertainties for coefficients of permeability and grain sizes; and, the tipping bucket model (Ligtenberg et al., 2018; Munneke et al., 2014) disregards the complex physics governing flow of water through it's own solid matrix, simplifying the problem to just density and cold content and assuming the flow of meltwater is instantaneous.

With firn advection tending to move open pore space underneath an increasingly melting surface, the depth/quantity of infiltration is key: the deeper melt penetrates, the more the pore space is 'overprinted' by surface melt and the advected deep pore space is not preserved. Alternatively, infiltration that is limited to shallow depths enhances the disparity between deep firn and that nearer to the surface. Our suite of model runs show that, in the lower percolation zone, the choice of infiltration scheme has nearly equivalent impact on the total air content as the incorporation of ice flow. Further understanding of the complex interplay between infiltration and firn transport is limited by poor knowledge and ability to simulate deep melt infiltration/refreezing physics. However, viewed another way, our results illustrate that continued efforts to improve infiltration processes should honor the full motion field that establishes the framework through which meltwater flow occurs.

7.4.2 Melt Feature Stratigraphy

Records of the melt features in ice cores are an important tool for quantifying time-changes in surface melting of GrIS as climate warms (Koerner, 1977; Kameda et al., 1995; Higgins, 2012). At Crawford Point, Higgins (2012) measured an overall trend of increasing MFP from 1765-2007 of 0.08% per year. However, melt events prior to 1900 were minor and infrequent; the more recent trend from 1900-2007 therefore increases to 0.11% per year. The advection signal we calculate is also highly dependent on the defined time period, but for a much different reason: different time periods sample different spatial gradients in climate as firn moves through the percolation zone. In recent decades, the MFP signal is not influenced by advection because local topography is essentially flat. However, over the ~100 years during which Higgins observes a significant increase in melt, our modeling suggests that approximately one third is attributable to the advection process. Thus, the stratigraphy of melt features along an ice core from the percolation zone can have a spatial component that must be evaluated to properly interpret temporal change.

That profiles of firn density and temperature are barely impacted by advection at Crawford Point, yet the MFP record is strongly influenced by advection, may seem counterintuitive. However, these are different entities: the former firn properties evolve over a time-space continuum, whereas the MFP record represents a time-trend in the occurrence of discrete events. Furthermore, the magnitude of trends sets the importance of advection in a MFP record. In the Crawford case, the multi-decadal trend in MFP due to changing melt is a fraction of a percent per year, an important indicator of changing climate, but not large enough to completely mask advection. Where the advection signal is strong it may be likely that it equivalent to the climate trend. Finally, this example demonstrates the impacts of km length scale topography in the

percolation zone: no advection signal was introduced to the youngest MFP record due to a locally flat region above Crawford Point.

Considering the potential for ice flow to obscure climate trends in measured firn cores, a simple procedure for quantifying this effect has utility. If the present ice sheet state (speed, accumulation, and melt rates) is assumed to be constant in time, an apparent climate signal at any core site can be quantified from spatially extensive datasets of the above variables. At a core depth corresponding to some time from present (t), the firn package originated at a location (x) upglacier from the core location, where x is the integral of the spatially varying velocity along the flowline over t years:

$$x(t) = -\int_0^t v(x)\, dt. \tag{1}$$

The MFP at this time (t) can be determined from the accumulation and melt conditions at this upglacier location:

$$MFP(x) = \frac{m(x)}{b(x)}. \tag{2}$$

Equations 1 and 2 can thus be combined to generate a time series of MFP which apparently reflects a changing climate, but actually records a spatially varying climate advected by ice flow.

7.5 Conclusion

Elevated horizontal ice flow in the percolation zone compared to ice divides results in a firn column that is not always well represented by 1D models for time-evolving density and temperature. The impacts of advection are highly variable around the ice sheet, but accounting

for advection in simulations can change the firn's air content by 10s of percent and the temperature can differ by several degrees. Lower accumulation, higher velocity, higher melt, and steeper topography (which drives climate gradients) all increase the mismatch between surface and deep conditions (and the failure of a 1D simulation). The advection process thus has greatest influence on firn evolution in the lower accumulation zone (e.g., 10-15 km); the conditions that are likely migrating upward as climate warms but are also subject to the greatest uncertainty regarding melt infiltration processes.

The 2D evolution of firn in the percolation zone is influenced by topography: horizontally invariant firn is generated in flat regions and hummocks/swales enhance the 2D influences from advection. The deeper meltwater penetrates, the more pore space is filled by surface melt and the advected deep pore space and cold content is not preserved. The stratigraphy of melt features along an ice core from the percolation zone can have a strong spatially derived component. Melt feature stratigraphy can be impacted by advection high in the percolation zone, where firn density and temperature are relatively unaffected by ice flow. This effect must be evaluated to properly interpret temporal changes in ice cores related to climate, especially over decadal and longer time scales.

8 References

Abdalati, W., & Steffen, K. (1997). Snowmelt on the Greenland Ice Sheet as Derived from Passive Microwave Satellite Data. *Journal of Climate*, *10*, 165–175.

Angelen, J. H. Van, Lenaerts, J. T. M., Broeke, M. R. Van Den, & Fettweis, X. (2013). Rapid loss of firn pore space accelerates 21st century Greenland mass loss, *Geophysical Research Letters*, *40*, 2109–2113. doi.org/10.1002/grl.50490

Arthern, R.J. and Wingham, D. J. (1998). The natural fluctuations of firn densification and their

effec on the geodetic determination of ice sheet mass balance, *Climatic Change, 40*, 605–624.

Arthern, R. J., Vaughan, D. G., Rankin, A. M., Mulvaney, R., & Thomas, E. R. (2010). In situ measurements of Antarctic snow compaction compared with predictions of models. *Journal of Geophysical Research*, *115*, 1–12. doi.org/10.1029/2009JF001306

Braithwaite, R. J., Laternser, M., & Pfeffer, W. T. (1994). Variations of near-surface firn density in the lower accumulation area of the Greenland ice sheet, Pakitsoq, West Greenland. *Journal of Glaciology*, *40*(136), 477–485. doi.org/10.1088/0022-3727/48/32/325305

Van Den Broeke, M. R., Enderlin, E. M., Howat, I. M., Kuipers Munneke, P., Noël, B. P. Y., Jan Van De Berg, W., et al. (2016). On the recent contribution of the Greenland ice sheet to sea level change. *Cryosphere*, *10*(5), 1933–1946. doi.org/10.5194/tc-10-1933-2016

Brown, J., Bradford, J., Harper, J., Pfeffer, W. T., Humphrey, N., & Mosley-Thompson, E. (2012). Georadar-derived estimates of firn density in the percolation zone, western Greenland ice sheet. *Journal of Geophysical Research: Earth Surface*, *117*(1). doi.org/10.1029/2011JF002089

Chylek, P., Dubey, M. K., & Lesins, G. (2006). Greenland warming of 1920 – 1930 and 1995 – 2005, *Geophysical Research Letters, 33*, 1–5. doi.org/10.1029/2006GL026510

Coléou, C., & Lesaffre, B. (1998). Irreducible water saturation in snow: experimental results in a cold laboratory. *Annals of Glaciology*, *26*(2), 64–68. doi.org/10.3189/1998AoG26-1-64-68

Ettema, J., Van Den Broeke, M. R., Van Meijgaard, E., Van De Berg, W. J., Bamber, J. L., Box, J. E., & Bales, R. C. (2009). Higher surface mass balance of the Greenland ice sheet revealed by high-resolution climate modeling. *Geophysical Research Letters*, *36*(12), 4–8. doi.org/10.1029/2009GL038110

Fausto, R. S., Ahlstrøm, A. P., Van As, D., Johnsen, S. J., Langen, P. L., & Steffen, K. (2009). Improving surface boundary conditions with focus on coupling snow densification and meltwater retention in large-scale ice-sheet models of Greenland. *Journal of Glaciology*, *55*(193), 869–878. doi.org/10.3189/002214309790152537

Fettweis, X., Tedesco, M., Van Den Broeke, M., & Ettema, J. (2011). Melting trends over the Greenland ice sheet (1958-2009) from spaceborne microwave data and regional climate models. *Cryosphere*, *5*(2), 359–375. doi.org/10.5194/tc-5-359-2011

Fettweis, X, Franco, B., Tedesco, M., Angelen, J. H. Van, Lenaerts, J. T. M., Broeke, M. R. Van Den, & Gall, H. (2013). Estimating the Greenland ice sheet surface mass balance contribution to future sea level rise using the regional atmospheric climate model MAR. *The Cryosphere*, 469–489. doi.org/10.5194/tc-7-469-2013

Fettweis, Xavier, Box, J. E., Agosta, C., Amory, C., Kittel, C., Lang, C., et al. (2017). Reconstructions of the 1900 – 2015 Greenland ice sheet surface mass balance using the

regional climate MAR model, *The Cryosphere, 11,* 1015–1033. doi.org/10.5194/tc-11-1015-2017

Forster, R. R., Box, J. E., Van Den Broeke, M. R., Miège, C., Burgess, E. W., Van Angelen, J. H., et al. (2014). Extensive liquid meltwater storage in firn within the Greenland ice sheet. *Nature Geoscience*, *7*(2), 95–98. doi.org/10.1038/ngeo2043

Graeter, K. A., Osterberg, E. C., Ferris, D. G., Hawley, R. L., Marshall, H. P., Lewis, G., et al. (2018). Ice Core Records of West Greenland Melt and Climate Forcing. *Geophysical Research Letters*, *45*(7), 3164–3172. doi.org/10.1002/2017GL076641

Hanna, E., Huybrechts, P., Cappelen, J., Steffen, K., Bales, R. C., Burgess, E., et al. (2011). Greenland Ice Sheet surface mass balance 1870 to 2010 based on Twentieth Century Reanalysis , and links with global climate forcing, *Journal of Geophysical Research, 116*, 1–20. doi.org/10.1029/2011JD016387

Harper, J., Humphrey, N., Pfeffer, W. T., Brown, J., & Fettweis, X. (2012). Greenland ice-sheet contribution to sea-level rise buffered by meltwater storage in firn. *Nature*, *491*(7423), 240–243. doi.org/10.1038/nature11566

Helm, V., Humbert, A., & Miller, H. (2014). Elevation and elevation change of Greenland and Antarctica derived from CryoSat-2, *The Cryosphere, 8*, 1539–1559. doi.org/10.5194/tc-8-1539-2014

Herron, M. M., & Langway, C. C. (1980). Firn densification: an empirical model. *Journal of Glaciology*, *25*(93).

Higgins, L. (2012). Construction and Analysis of an Ice Core-Derived Melt History from West Central Greenland (1765-2006), (Masters thesis). Columbus, OH: University of Ohio.

Humphrey, N. F., Harper, J. T., & Pfeffer, W. T. (2012). Thermal tracking of meltwater retention in Greenland's accumulation area. *Journal of Geophysical Research: Earth Surface*, *117*(1), 1–11. doi.org/10.1029/2011JF002083

Janssens, I., & Huybrechts, P. (2000). The treatment of meltwater retention in mass-balance parameterizations of the Greenland ice sheet. *Annals of Glaciology*. doi.org/10.3189/172756400781819941

Joughin, I., Smith, B. E., Howat, I. M., Scambos, T., & Moon, T. (2010). Greenland flow variability from ice-sheet wide velocity mapping. . *Journal of Glaciology*, *56*(197), 415–430.

Kameda, T., Narita, H., Shoji, H., Nishio, F., Fujii, Y., & Watanabe, O. (1995). Melt features in ice cores from Site J, southern Greenland: some implications for summer climate since AD 1550. *Annals of Glaciology*, *21*, 51–58. doi.org/https://doi.org/10.1017/S0260305500015597

Koenig, L. S., Miège, C., Forster, R. R., & Brucker, L. (2014). Initial in situ measurements of perennial meltwater storage in the Greenland firn aquifer, *Geophysical Research Letters, 41*, 81–85. doi.org/10.1002/2013GL058083

Koerner, R. M. (1977). Devon Island Ice Cap: Core Stratigraphy and Paleoclimate. *Science*, *196*(4285).

Li, J, & Zwally, H. J. (2002). Modeled seasonal variations of firn density induced by steady state surface air temperature cycle. *Annals of Glaciology*, 299–302. doi.org/10.3189/172756402781817707

Li, Jun, & Zwally, H. J. (2004). Modeling the density variation in the shallow firn layer. *Annals of Glaciology*, *38*, 309–313. doi.org/10.3189/172756404781814988

Ligtenberg, S R M, Helsen, M. M., & Broeke, M. R. Van Den. (2011). The Cryosphere An improved semi-empirical model for the densification of Antarctic firn. *The Cryosphere*, *5*, 809–819. doi.org/10.5194/tc-5-809-2011

Ligtenberg, Stefan R.M., Munneke, P. K., Noël, B. P. Y., & Van Den Broeke, M. R. (2018). Brief communication: Improved simulation of the present-day Greenland firn layer (1960-2016). *Cryosphere*, *12*(5), 1643–1649. doi.org/10.5194/tc-12-1643-2018

Lundin, J. M. D., Stevens, C. M. A. X., Arthern, R., Buizert, C., Orsi, A., Ligtenberg, S. R. M., et al. (2017). Firn Model Intercomparison Experiment (FirnMICE). *Journal of Glaciology*, *63*, 401–422. doi.org/10.1017/jog.2016.114

MacGregor, J. A., Colgan, W. T., Fahnestock, M. A., Morlighem, M., Catania, G. A., Paden, J. D., & Gogineni, S. P. (2016). Holocene deceleration of the Greenland Ice Sheet. *Science*, *351*(6273).

Machguth, H., MacFerrin, M., van As, D., Box, J. E., Charalampidis, C., Colgan, W., et al. (2016). Greenland meltwater storage in firn limited by near-surface ice formation. *Nature Climate Change*, *6*(4), 390–393. doi.org/10.1038/nclimate2899

Meehl, G., Washington, W., Arblaster, J., Hu, A., Teng, H., & Tebaldi, C. (2012). Climate System Response to External Forcings and Climate Change Projections in CCSM4. *Journal of Climate*, *25*, 3661–3683. doi.org/10.1175/JCLI-D-11-00240.1

Meyer, C. R., & Hewitt, I. J. (2017). A continuum model for meltwater flow through compacting snow. *Cryosphere*, *11*(6), 2799–2813. doi.org/10.5194/tc-11-2799-2017

Mote, T. L. (2007). Greenland surface melt trends 1973-2007: Evidence of a large increase in 2007. *Geophysical Research Letters*, *34*(22), 1–5. doi.org/10.1029/2007GL031976

Munneke, P. K., Ligtenberg, S. R. M., Van Den Broeke, M. R., Van Angelen, J. H., & Forster, R. R. (2014). Explaining the presence of perennial liquid water bodies in the firn of the Greenland Ice Sheet. *Geophysical Research Letters*, *41*(2), 476–483.

doi.org/10.1002/2013GL058389

Noël, B., Berg, W. J. Van De, Wessem, J. M. Van, Meijgaard, E. Van, & As, D. Van. (2018). Modelling the climate and surface mass balance of polar ice sheets using RACMO2 – Part 1 : Greenland (1958 – 2016), *The Cryosphere, 12*, 811–831.

Paterson, W. S. B. (1994). *The Physics of Glaciers* (3rd ed.). Elsevier.

Pfeffer, W. T. A. D., Memr, M. F., Pfeffer, W. T., Meier, M. F., & Illangasekare, T. H. (1991). Retention of Greenland runoff by refreezing: Implications for projected future sea level change. *Journal of Geophysical Research*, *96*(C12), 22117. doi.org/10.1029/91JC02502

Reeh, N., Fisher, D. A., Koerner, R. M., & Clausen, H. B. (2005). An empirical firn-densification model comprising ice lenses. *Annals of Glaciology*, *42*, 101–106. doi.org/10.3189/172756405781812871

Reijmer, C. H., Van Den Broeke, M. R., Fettweis, X., Ettema, J., & Stap, L. B. (2012). Refreezing on the Greenland ice sheet: A comparison of parameterizations. *Cryosphere*, *6*(4), 743–762. doi.org/10.5194/tc-6-743-2012

Rignot, E., & Kanagaratnam, P. (2006). Changes in the Velocity Structure of the Greenland Ice Sheet. *Science*, *311*, 986–991.

Robin, G. de Q. (1958). *Glaciology III: Seismic Shooting and related investigations*. Norsk Polarinstitutt.

Simonsen, S. B., Stenseng, L., Aðalgeirsdo, G., Fausto, R. S., Hvidberg, C. S., & Lucas-picher, P. (2013). Assessing a multilayered dynamic firn-compaction model for Greenland with ASIRAS radar measurements. *Journal of Glaciology*, *59*(215), 545–558. doi.org/10.3189/2013JoG12J158

Steger, C. R., Reijmer, C. H., Broeke, M. R. Van Den, Wever, N., Lhermitte, S., Ligtenberg, S. R. M., et al. (2017). Firn Meltwater Retention on the Greenland Ice Sheet : A Model Comparison, *Front. Earth Sci, 5(3)*. https://doi.org/10.3389/feart.2017.00003

Tedesco, M. (2007). Snowmelt detection over the Greenland ice sheet from SSM/I brightness temperature daily variations. *Geophysical Research Letters*, *34*(2), 1–6. doi.org/10.1029/2006GL028466

Tedesco, M., Fettweis, X., Mote, T., Wahr, J., Alexander, P., Box, J.E., & Wouters, B. (2013). Evidence and analysis of 2012 Greenland records from spaceborne observations, a regional climate model and reanlysis data. *The Cryosphere, 7,* 615-630. doi.org/10.5194/tc-7-615-2013

Trusel, L. D., Das, S. B., Osman, M. B., Evans, M. J., Smith, B. E., Fettweis, X., et al. (2018). Nonlinear rise in Greenland runoff in response to post-industrial Arctic warming. *Nature*,

564(7734), 104–108. doi.org/10.1038/s41586-018-0752-4

Vandecrux, B., Fausto, R. S., Langen, P. L., As, D. Van, & Macferrin, M. (2018). Drivers of Firn Density on the Greenland Ice Sheet Revealed by Weather Station Observations and Modeling, *Journal of Geophysical Research: Earth Surface, 123.* doi.org/10.1029/2017JF004597

Vizcaino, M., Mikolajewicz, U., Ziemen, F., Rodehacke, C. B., Greve, R., & Broeke, M. R. (2015). Coupled simulations of Greenland Ice Sheet and climate change up to A.D. 2300, *Geophysical Research Letters, 42,* 3927–3935. doi.org/10.1002/2014GL061142

Van De Wal, R. S. W., Boot, W., Van Den Broeke, M. R., P. Smeets, C. J. P., Reijmer, C. H., Donker, J. J., et al. (2008). Large and Rapid Melt-Induced Velocity Changes in the Ablation Zone of the Greenland Ice Sheet. *Science*, *321*, 111–114.

Yi, D., Zwally, H. J., & Sun, X. (2005). ICESat measurement of Greenland ice sheet surface slope and roughness, *Annals of Glaciology, 42,* 83–89.

Zwally, H. J., & Jun, L. (2002). Seasonal and interannual variations of firn densification and ice-sheet surface elevation at the Greenland summit. *Journal of Glaciology*, *48*(161), 199–207. https://doi.org/10.3189/172756502781831403

Zwally, H. J., Li, J., Brenner, A. C., Beckley, M., Cornejo, H. G., Dimarzio, J., et al. (2011). Greenland ice sheet mass balance : distribution of increased mass loss with climate warming ; 2003 – 07 versus 1992 – 2002, *Journal of Glaciology, 57*(201), 88–102.